Geomorphological and geological controls on storage-discharge functions of Alpine landscapes: evidence from streamflow analysis in the Swiss Alps and perspectives for the Critical Zone Community

Clément Roques[1,2], Sibylle Lacroix[2], Kerry Leith[2], Laurent Longuevergne[1], Sarah Leray[3], Elisabeth R. Jachens[4], David E. Rupp[5], Jean-Raynald de Dreuzy[1], Nicolas Cornette[1], Larissa B. de Palézieux[2], Nicolas Oestreicher[2], Alexandre Boisson[6], Gordon Grant[7], and John S. Selker[4]

[1]Univ Rennes, CNRS, Geosciences Rennes, UMR 6118, 35000 Rennes, France.

[2]Department of Earth Sciences, Institute of Geology, ETH Zürich, Zürich, Switzerland.

[3]Departamento de Ingeniería Hidráulica y Ambiental, Pontificia Universidad Católica de Chile, Santiago, RM, Chile

[4]Department of Biological and Ecological Engineering, Oregon State University, Corvallis, Oregon, USA

[5]Oregon Climate Change Research Institute, College of Earth, Ocean, and Atmospheric Sciences, Oregon State University, Corvallis, Oregon, USA

[6]BRGM DAT Bretagne, Rennes Atalante Beaulieu, 2 rue de Jouanet, 35700 Rennes, France

[7]USDA Forest Service, Pacific Northwest Research Station, Oregon State University, Corvallis, Oregon, USA

Corresponding author: Clément Roques (clement.roques@univ-rennes1.fr or roquesclem@gmail.com)

Key Points:

- Catchment recession is influenced by non-linear processes due to heterogeneity of mechanisms controlling storage-discharge relations;
- These non-linearities raise questions about applying homogeneous assumptions (i.e., Bousinessq) when modeling catchment behavior;
- Considering lithological constraints alone do not allow description of the interactions between the subsurface and streamflow dynamics;
- Geomorphological and hydrological processes coevolve in shaping groundwater flow architectures and controlling storage-discharge relations.

Abstract

Predicting the impact of changing climate and anthropogenic influences on stream discharge dynamics and baseflow conditions requires insight into the main factors that regulate storage and transfer of water from hillslope aquifers to surface streams. Classically, it is assumed that above a certain scale, hydrological laws involved at small-scale can be simplified, allowing the representation of the landscape and its subsurface in models as a homogeneous hillslope with effective slope, length and hydraulic properties. From a comprehensive analysis of hydrological, geological and geomorphological databases available in the Swiss Alps we provide evidence that such simplification might lead to inaccurate estimates of streamflow dynamics at baseflow. We reveal that recession behavior strongly deviates from that predicted by idealized homogeneous theories. A correlation analysis allows us to identify which key features of the landscape might control this deviation, with particular attention to slope, drainage density, depth to bedrock, and lithology as the main drivers. We summarize the current knowledge of physical mechanisms that could lead to complex hydrological behavior in Alpine contexts, and we finally discuss implications in defining modeling strategies for the Critical Zone community.

Plain Language Summary

In introductory courses in hydrology, geomorphology, and geology, we learn that water flowing through the landscape weathers rocks that, in turn, influence the pathways by which water flows through the landscape. We also learn that the movement of water through the landscape carves and shapes that landscape, and that the shape of the landscape, in turn, changes the architecture of the hydrological cycle. Current hydrological models build to assess groundwater storage and streamflow behavior at regional to global scales tend to neglect this evolving architecture, representing the subsurface as a box with homogeneous properties where lithology is the main constraint on hydraulic properties. Based on the analysis of streamflow recessions across 54 catchments in the swiss Alps we discuss the strong limitations raising from this assumption. We propose original hypothesis on the role of geomorphological processes in controlling the distribution of the water resources availability in space and time.

1 INTRODUCTION

Water is ubiquitous, being both a key component sustaining life, and a key actor for weathering, transporting energy and nutrients (Richter and Billings, 2015). As a liquid, water flows from high to low altitudes, at the surface and the subsurface, connecting and structuring different elements of our landscapes. Several recent studies have underscored the strong coupling between water and carbon cycles (Gentine et al., 2019), in which water availability, more than temperature, might be a dominant driver of ecological systems at local and interannual time scales (Jung et al., 2017). Understanding the processes that regulate how our landscapes store and release water into the stream network has been identified by the hydrological community as a major challenge (Blöschl et al., 2019), while being central to questions of the Critical Zone community (Fan, 2015; Fan et al., 2019; Gaillardet et al., 2018; Riebe et al., 2017). Such knowledge is essential for evaluating the resilience of hydrological systems to extended drought periods, planning for appropriate human activities, and anticipating the impact of global changes on water resources. Evaluating the influence of groundwater on stream dynamics is key (Alley et al., 2002; Taylor et al., 2013), but requires systematic quantification based on uncertain boundary conditions and state variables without elaborate calibration (Abbott et al., 2019). The hidden and cryptic nature of groundwater makes this a daunting challenge.

The storage and transfer of water across landscapes is controlled by a range of interconnected factors operating and possibly coupled at various scales, including plant interception, geomorphology, soil properties, geological heterogeneity and rainfall variability. Considering the wide range of spatial scales required to define water transfer (from leaf to basin), hydrological modeling strategies at catchment, regional and global scales rely on simplified assumptions to integrate the effects of surface and subsurface heterogeneities below a representative elementary area (Wood et al., 1988). In this context, the hillslope is classically considered as the elementary entity (Fan, 2015), where processes are characterized by effective geometric and hydrodynamic properties. However, studies have questioned such simplifications, which might introduce strong limitations in predicting streamflow dynamics, especially during baseflow (Clark et al., 2009). Simplifying or even neglecting processes may result in prediction errors, independent of the scale considered, such as interbasin fluxes (Liu et al., 2020), spatial and vertical distribution of flow paths (Clark et al., 2009; Harman et al., 2009; Rupp and Selker, 2005), influence of planform shape of elementary area on flow paths

(Paniconi et al., 2003), and spatial variability of recharge and evapotranspiration (Hartmann et al., 2017; Jachens et al., 2020; Tashie et al., 2019). This leads to two motivating questions: 1) in which geological and geomorphological contexts are simplified effective representations likely to fail to describe water storage-discharge dynamics? And 2) conversely, in which contexts are such simplifications still acceptable? Evidence from field observations is required to address these questions, and in turn, define relevant physical laws and parameterization of regional scale storage-discharge relations (Clark et al., 2017; Fan et al., 2019).

In this study, we test two complementary hypotheses regarding the potential controls of landscape heterogeneity on storage-discharge behavior. In the first hypothesis, we consider a representative elementary area smaller than the hillslope scale, and posit that storage-discharge processes involved at the catchment scale are not significantly influenced by landscape and subsurface heterogeneities. Stream baseflow dynamics can then be obtained from an aquifer represented by an effective reservoir whose hydraulic properties can be constrained from lithological properties (Clark et al., 2015; Gleeson et al., 2011; Kollet and Maxwell, 2006; Schaller and Fan, 2009). In the second hypothesis, we evaluate the contribution of landscape and sub-surface heterogeneity (including stream drainage organization, topographic slope, soil development and geology) to the storage-discharge relationship at the catchment scale heterogeneity (Biswal and Nagesh Kumar, 2015; Jefferson et al., 2010; Rempe and Dietrich, 2014; Yoshida and Troch, 2016). We test these hypotheses by exploring the relationship between landscape characteristics (spatial variability and correlation structure) and their storage-discharge functions, taking advantage of the combined hydrological and geophysical information available in regional datasets. We focus our analysis on catchments located in the well-instrumented Swiss Alps because of the variety of landscape and geological configurations. We summarize several hypotheses on the potential controlling factors of streamflow recession, as supported by a review of the literature. We finally draw some conclusions and perspectives for the representations of subsurface water flow for large-scale modeling strategies.

2 CONTEXT AND DATA

2.1 THEORETICAL BACKGROUND FOR HOMOGENEOUS AQUIFERS

Streamflow recession analysis is commonly used to estimate the storage-discharge functions of catchments. This method is based on the analysis of the falling limb of the hydrograph after a precipitation event. Saturated-flow theory (for horizontal homogeneous aquifers) predicts that the rate of change in discharge of an aquifer to a stream scales with the actual discharge following a power law relationship (Brutsaert and Nieber, 1977).

$$\frac{-dQ}{dt} = a\,Q^{b} \qquad \text{Eq. 1}$$

where a and b are recession constants that can be related to geometric and hydraulic properties of the aquifer system under predominately diffusive or kinematic flow and idealized geometry (Rupp and Selker, 2006). b is specifically defined as the constant of non-linearity in the storage-discharge function (Kirchner, 2009). A watershed's capacity to maintain late-season streamflow is tightly linked to b (Figure 1b and c), wherein a resilient stream will have large values of b (Berghuijs et al., 2016; Jachens et al., 2020; Kirchner, 2009). In real catchments, b has been shown to vary over a wide range of values, - from ~1 to greater than 10 (Tashie et al., 2020). Reference models for homogeneous and horizontal aquifers theoretically predict values from 1 to 3, following the "early" and "late" time solutions derived from the Boussinesq solutions. Under low flow conditions, $b=1$ in the case of constant aquifer transmissivity (i.e. where changes in the saturated thickness are negligible), and $b=1.5$ for a homogeneous unconfined aquifer (Brutsaert and Nieber, 1977; Rupp and Selker, 2006; Troch et al., 2013). For an unconfined aquifer, values larger than 1.5 mark deviations from the homogeneous model that may come from heterogeneous geological and geomorphological conditions, for example an aquifer with decreasing hydraulic conductivity with depth (Rupp and Selker, 2005), or lateral heterogeneity in hydraulic properties (Harman et al., 2009).

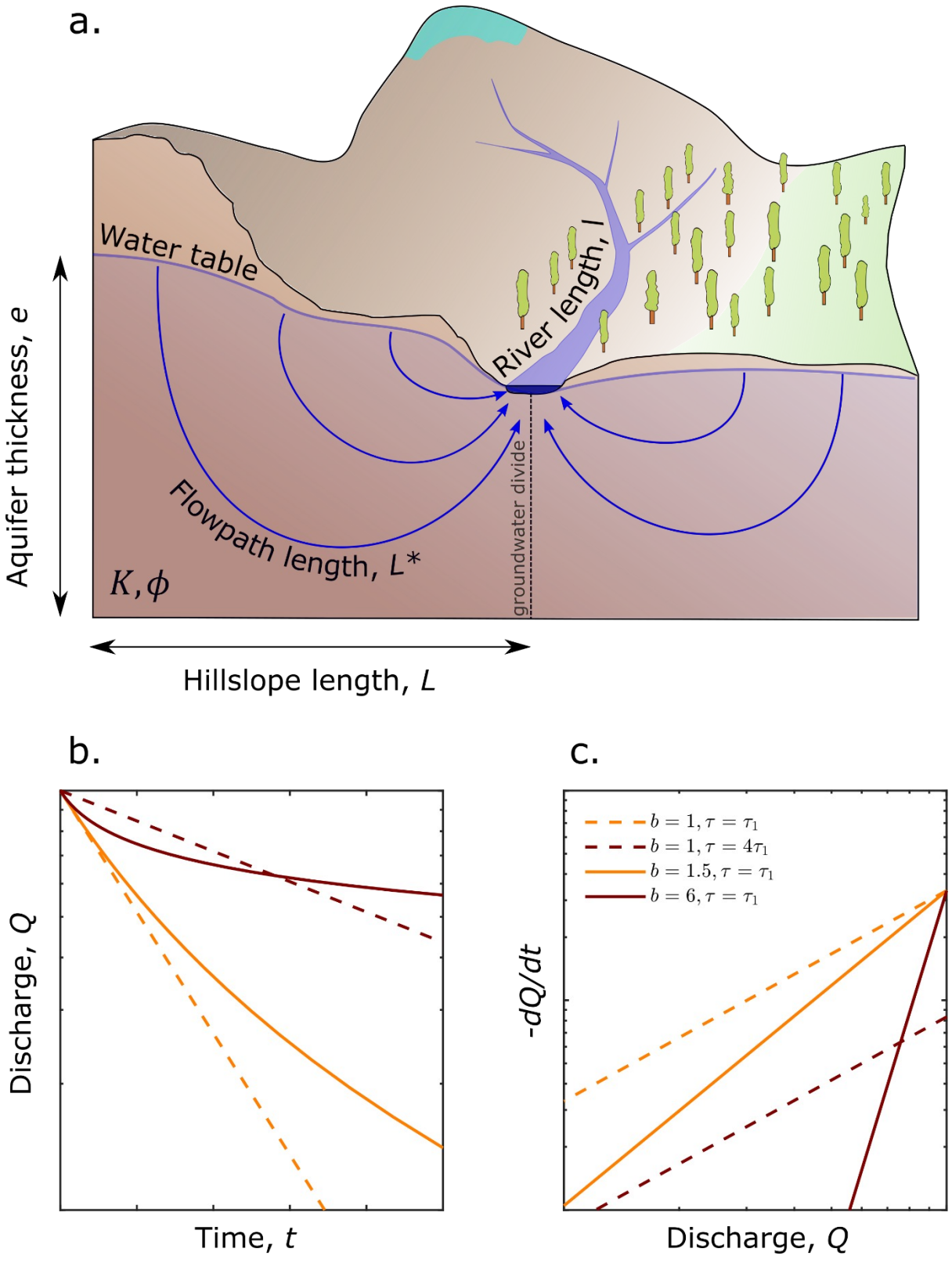

Figure 1. a. Conceptual representation of a hillslope from ridge to stream, in which the water table follows topography, and groundwater flow paths are organized from the recharge zone to discharge at the stream. The main metrics used in the manuscript are defined. K and φ stand for hydraulic conductivity and porosity respectively. b. Typical

150 **streamflow hydrographs for different values of recession timescale τ and constant of**
151 **non-linearity b. The Y axis is in log scale. In c. are drawn the recession plots $-dQ/dt$ vs**
152 **Q for the 4 hydrographs presented in b. Both X and Y axes are in log scales. Values of t,**
153 **Q, and τ in b. and c. are arbitrary.**

154 From the linear solution with $b=1$, the characteristic diffusion timescale, $\tau=1/a$, can be
155 defined as being proportional to the square of the characteristic flow path length $L[m]$
156 divided by the diffusivity, $D[m^2/s]$ (the ratio of the transmissivity $T[m^2/s]$ by the porosity
157 φ: KH/ϕ, H is the aquifer thickness) of the aquifer connected to the stream (Brutsaert &
158 Lopez, 1998). τ represents the half-life of storage (for $b=1$) so that for higher values of τ, the
159 rate of change in discharge is lower so that discharge extend over a longer period than lower
160 values of τ (Figure 1b and c). Drainage timescale has been estimated analytically by Brutsaert
161 (1994) as:

$$\tau=\frac{1}{a}, with\ a=\left[\frac{KH}{\phi}\right]\left[\frac{\pi^2 p l^2}{A^2}cos\beta\right]\left[1+\left(\frac{\eta}{\pi p}\right)^2\right] \qquad \text{Eq. 2?}$$

162

163 where the first term between brackets represents the geological effect, where K and φ are the
164 mean hydraulic conductivity and porosity, respectively; the second term represents the
165 geomorphological influence, where β the slope angle, A the catchment area, and l the total
166 stream network length (Figure 1). p is an empirical weighting factor generally taken between
167 0.1-0.3 (Brutsaert, 2008, 1994). In the following we consider an average value with $p=0.2$.
168 Finally, the third term includes the effect of slope (Rupp and Selker, 2006), with $\eta=B\,tan\beta$, B
169 being the characteristic hillslope length from stream to ridge.

170 This mathematical framework allows an estimation of the key geometrical and hydraulic
171 properties of the landscape and its subsurface. In this study we characterize hydrological
172 behavior by evaluating the spatial variations of both τ and b with respect to a range of metrics
173 relating to catchment heterogeneity.

174 2.2 DISCHARGE DATA

175 We analyzed daily discharge time series measured from stream gauging stations maintained
176 by the Swiss Federal Office for the Environment (FOEN). The selection of the watersheds
177 was inspired by previous studies performed in the same area (Birsan et al., 2005; Clara

178 Santos et al., 2018) to which additional watersheds have been considered in order to cover a
179 greater range of geomorphological and geological settings. We have selected gauging stations
180 that have at least 30 years of continuous record and excluded those that could be influenced
181 by extended lakes and the presence of potential anthropogenic regulations such as dams.
182 These were identified through a careful analysis of national maps, aerial photographs, and a
183 global database of reservoirs and dams.

184 We also checked for evidence in the discharge time series of regulation practices by looking
185 at the presence of typical step-like changes in discharge at low flows. These criteria resulted
186 in the selection of the 54 watersheds displayed in Figure 4 with a diversity of flow regimes,
187 i.e., rain-, snow- and glacier-dominated regimes (Birsan et al., 2005).

188 2.3 LANDSCAPE PROPERTIES

189 We used the digital elevation model DHM25 GeoVite of Switzerland provided by the Federal
190 Office of Topography to compute landscape properties previously identified in Eq. 2 (Figure
191 2a. and b.). The DEM has lateral resolution of 25 m and vertical accuracy of 1.5 m for the
192 plains and the Jura, 2 m for the pre-Alps and Canton Ticino, and 3 m for the central Alps. The
193 global lithological dataset GLiM (Hartmann and Moosdorf, 2012) was used for the
194 lithological classification. The lithological units were classified into 5 main units:
195 unconsolidated sediments, sedimentary, volcanic, plutonic and metamorphic rocks (Figure
196 4a).

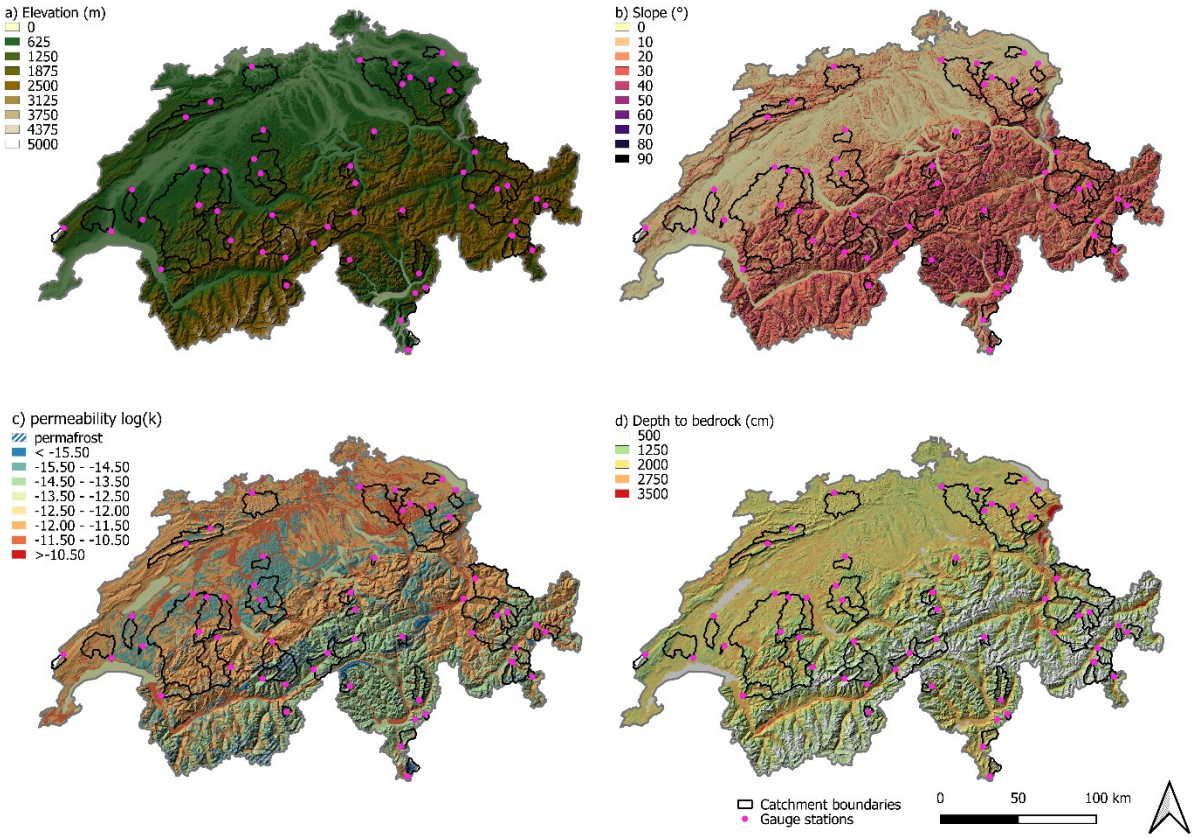

197

198 **Figure 2. Maps of the Swiss Alps with a) elevation, b) slopes, c) permeability values (m2)**
199 **in log scale extracted from the GLHYMPS database** (Huscroft et al., 2018)**, and, d) the**
200 **depth to bedrock** (Shangguan et al., 2017)**.**

201 The geometry of the fluvial network was computed from the 25m resolution DEM using the
202 Arc Hydro Toolbox implemented in ArcGIS (ESRI, 2011). The total length of streams l, was
203 computed as the sum of the length of individual stream segments in a catchment. The
204 drainage density (ζ) was calculated as the total length of the streams in the watershed divided
205 by catchment area, $\zeta = l/A$.

206 Hydrogeological properties (Figure 2c), i.e., hydraulic conductivity and porosity K and φ, of
207 the subsurface were extracted from the global database GLHYMPS (Huscroft et al., 2018).
208 GLHYMPS provides values of permeability $k\left[m^2\right]$ that have been converted to hydraulic
209 conductivities $K = k\rho g/\mu$ assuming water properties where $\rho = 1000[kg/m^3]$ is the density of
210 water, μ=1e-3$[Pa.s]$ its density, and gravity $g = 9.8\,m/s^2$. If several hydrogeological units
211 were present in the watershed, we computed the geometric average of permeability and
212 porosity weighed by the area of each unit with respect to total catchment area. Variability (σ)

213 in K and $\varphi$where also computed as the geometric average of standard deviations of K and φ
214 also weighted as a function of the area of hydrogeological units.

215 We compiled information about depth to bedrock (DTB, Figure 2d) available in the Global
216 Depth to Bedrock Dataset for Earth System Modeling (Shangguan et al., 2017). Authors
217 defined the DTB as the '*depth from the ground surface to the contact with coherent*
218 *(continuous) bedrock.*' The layer covering the bedrock includes unconsolidated sediments,
219 soil and regolith. The map relied on three types of data sources: soil profiles, boreholes logs,
220 and soft and remote observations - i.e. remote sensing data or literature. The dataset has a
221 spatial resolution of 250m (Shangguan et al., 2017).

222 3 METHODOLOGY

223 3.1 STREAMFLOW RECESSION ANALYSIS

224 In order to determine the storage-discharge behaviour of the different catchments, we
225 performed streamflow recession analyses to estimate b and τ in two ways: 1) We estimated
226 the parameters from the ensemble of recessions (often called the 'cloud' of recessions) in
227 order to represent the average behavior (Brutsaert and Nieber, 1977; Kirchner, 2009); and 2)
228 We estimated the parameters for every single recession to examine the temporal variability
229 among recessions. For the analysis of the cloud, we used the binning and fitting approach
230 proposed by Kirchner (2009). For the single recession analysis, we used the method proposed
231 by Roques et al., (2017): we isolated segments in the stream discharge time series that
232 decrease monotonously between recharge events. Recharge events were defined as discharge
233 peaks that exceeded five times the absolute measurement accuracy, computed as the
234 minimum discharge drop measured in the entire time series. The first day after the peak was
235 excluded to reduce potential influence from the overland flow on the recession parameter
236 estimation (Dralle et al., 2017).

237 We distinguished high flows from the baseflow regimes by considering a threshold discharge,
238 set to the long-term median (Q_{50}). Although this value was arbitrarily set and has no specific
239 physical meaning, it offers a consistent methodology across the catchments. This
240 methodology presents the advantage if excluding periods in the discharge time series that are
241 dominated by strong recharge from rain, snow or glacier melt. This means that the recession
242 values for rain-dominated catchments are estimated during late summer and fall while for

243 catchments with snow and glacier melt regimes, estimates are made during winter when the
244 catchments are covered by snow and when streamflow is only controlled by groundwater
245 discharge (Andermann et al., 2012).

246 The recession derivative, $-dQ/dt$, was estimated using the Exponential Time Steps (ETS)
247 method proposed by Roques et al., (2017). The recession coefficients a and b in Eq. 1 were
248 determined using a linear least-squares regression on the log transformed data, i.e.,
249 $\log(-dQ/dt)$ vs $\log(Q)$ (Shaw and Riha, 2012).

250 The analysis included data from more than three decades for the 54 selected catchments. The
251 algorithm identified 54,000 recessions in total, among which 13,600 respected the selection
252 and quality criteria. This represents an average of 250 estimates per station. In the following
253 section, we describe how we computed the mean and standard deviation values of b_H , b_L (the
254 subscripts H and L stand for High and Low flow regimes, respectively) from a log-normal fit
255 on the distribution to avoid potential influence from outliers (Figure 3). In order to evaluate
256 the temporal variability of each parameter, we computed the coefficient of variations (
257 $CV=\sigma/\mu$, where σ is the standard deviation and μ is the mean). The precision of the mean
258 is assessed through the standard error as $\sigma/\sqrt{N}$ with N the number of samples.

259 ## 3.2 ESTIMATION OF RECESSION TIMESCALES AND HYDRAULIC PROPERTIES

260 We estimated the characteristic timescale τ from the low-flow groundwater-dominated
261 segments of the recessions (i.e.., for $Q_t<Q_{50}$) as $1/a$, and derived the effective hydraulic
262 properties of the catchments using Eq. 2 for the case of $b=1$ (exponential in Eq. 2). This
263 means that for each estimate of b_L (section 3.1) we also obtained an evaluation of τ. We then
264 compared fitted values of τ with those estimated analytically from Eq. 2 (Brutsaert, 1994)
265 accounting for the geometric and hydraulic properties extracted from the global databases
266 previously described.

267 ## 3.3 STATISTICAL ANALYSIS

268 Our main objective is to decipher the landscape factors controlling streamflow behaviour. For
269 this, we performed a cross-correlation analysis of hydrological and geomorphological
270 databases combining classical multivariate correlation approaches. We used a Principal
271 Component Analysis (PCA) to investigate the correlation structure among the ensemble of
272 the variables and isolate the main variable(s) controlling the variance in our dataset. We also

quantified the degree of correlation between each of the pairs of variables based on an analysis of the correlation matrix using Pearson's coefficient of determination r^2.

4 RESULTS

4.1 HYDROLOGICAL REGIMES AND LANDSCAPE CONTROLS

To visualize the extent to which landscape properties control streamflow dynamics, we consider annual hydrographs for three stations located in similar lithologies, i.e. crystalline rocks, and alpine settings (Figure 3). The basin morphologies pictured on the aerial photos (first row) show typical glacier morphological features on the left (Fig. 3a) while the basin on the right (Fig. 3c) is characterized by a fluvial-dominated morphology (with 20% coverage of alluvial deposits). The basin in the middle (Fig. 3b) is a hybrid with upland cirque features characteristic of montane glaciers and a fluvially incised valley. The three landscapes show distinct hydrological responses (second row in Figure 3) with most of the recharge happening during spring snow-melt and precipitation (de Palézieux and Loew, 2019). On the left-hand side, maximum discharge happens during spring and summer with a clear peak in July followed by a long recession timescale on which short term discharge events of low amplitude are superimposed. On the right-hand side, discharge in response to snow melt happens to be of lower magnitude with faster recession. Precipitation events induce sharper discharge responses. This highlights the fundamental difference in the storage-discharge functions across these landscapes, controlled by differences in recharge dynamics and subsurface flow processes, with a higher efficiency for drainage (higher subsurface diffusivity) in the case of the fluvially dominated landscape (right). This is particularly visible when looking at a specific hydrograph typical of a drought year, here 2003 in Figure 3. While discharge in the glacier-dominated landscape (left) remains in the 10-90th quantile range, discharge in the fluvial one (right) drops significantly below the 10th quantile.

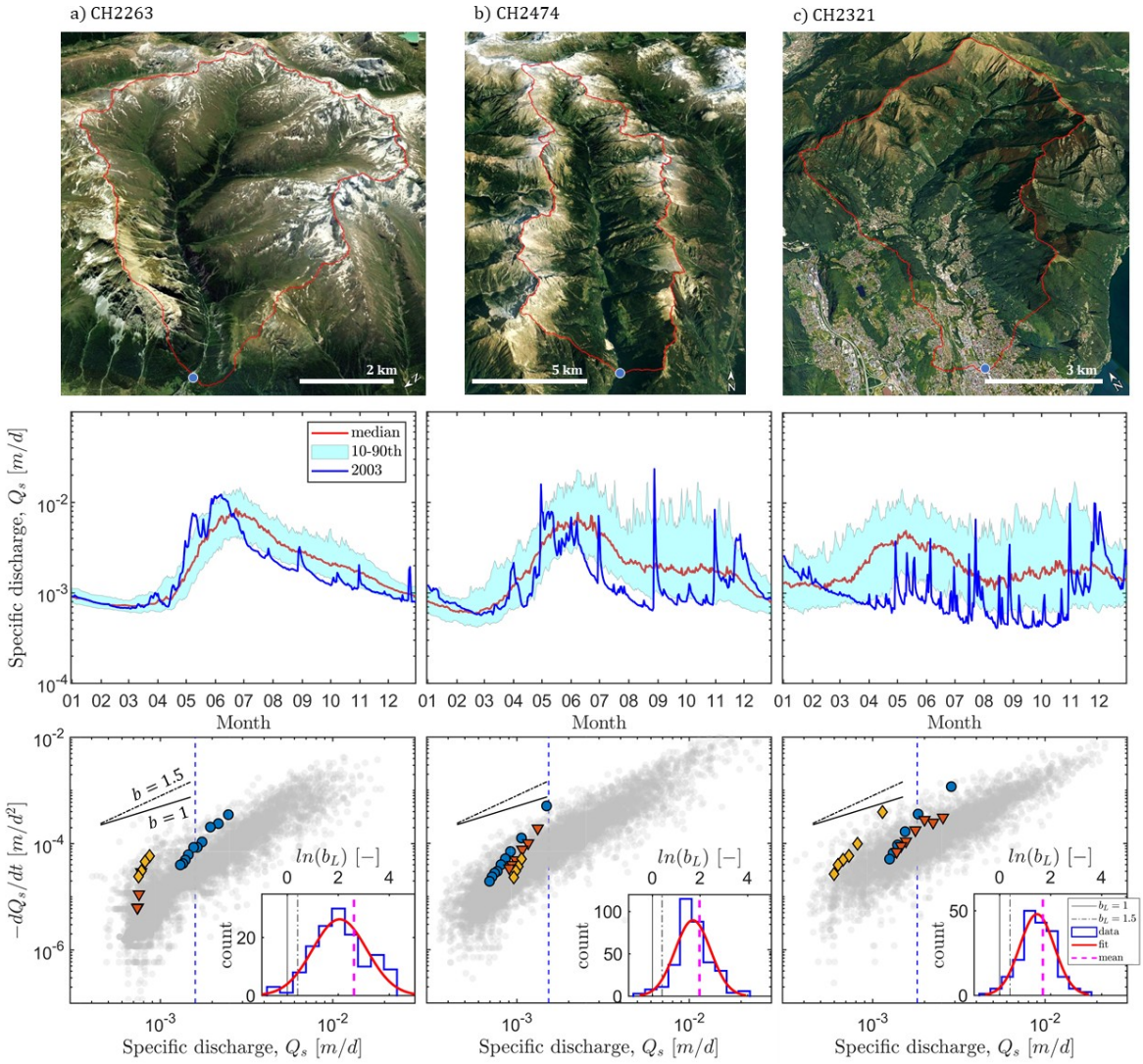

Figure 3. Typical contrasts in alpine bedrock landscapes, organized by columns, and their hydrological responses. The ID numbers used by the Swiss federal office are displayed on the top of the figure. The top row presents an aerial view of the catchments with their drainage area drawn with red contours and the location of the gauging station represented by blue dots. Pictures were taken in July 2014 for the left hand one and the 2 others are from October 2019. The middle row displays the annual hydrographs for the 3 watersheds with the 10-90th quantile range displayed as the shaded cyan band, the median flow with a red line and in blue the hydrograph for 2003 which was a year of intense drought in Europe. On the bottom row, the recession plots are shown as $-dQ_s/dt$ vs Q_s in a log-log space. Grey transparent points are the stacked recessions computed from the ETS method presented in section 3.1. We also display 3 examples of single recession events chosen randomly that are identified with blue,

orange, and yellow points. The vertical dashed lines represent the long-term median value of specific discharge that was used as the threshold to separate b_H estimated at high flows from b_L and τ estimated at low flows. Inserts show the histograms of $\ln(b_L)$ showing lognormal distributions. The red line represents the fitted distribution, while the magenta dashed line shows the mean value of $\ln(b_L)$ of the fitted distribution. Black continuous and dash-dotted lines serve as references for $b=1$ and $b=1.5$ respectively in both the main figure and the insert.

This difference is also visible in the recession plots (third row of Figure 3) displaying the rate of change in specific discharge, $-dQ_s/dt$, as a function of average specific discharge Q_s, in a bi-logarithmic scale. We highlight three individual recessions chosen randomly with different symbols and colors for each station to illustrate how the variability in responses operate across different recessions. For the glacier-dominated landscape (left), we notice the strong decrease in $-dQ_s/dt$ toward the lower discharge values which means the discharge is almost stabilizing. While for the fluvial dominated landscape (right), recessions do not show such stabilization with higher values of $-dQ_s/dt$ (stronger decrease in discharge over time). One may also notice that the variability in recession constants b_L seems to be greater in the case of the glacier-dominated landscape compared to the fluvial dominated one revealing stronger sensitivity to initial conditions prior to recession. This is confirmed in the histograms of b_L (inserts in Figure 3, third row) across the three catchments. All three histograms display lognormal distributions, i.e. $\ln(b_L)$ shows a normal-like distribution. Modes, means and variances of $\ln(b_L)$ evolve from higher values in the context of the glacier-dominated catchment toward lower ones in the fluvial dominated one.

We also draw attention to the pronounced differences visible between the individual recession power laws and the one from the cloud (grey dots). Similar to conclusions drawn from previous studies (Jachens et al., 2020; Tashie et al., 2020), it shows that single recessions do not follow the same laws as the lower envelope of the cloud of recessions and, by including other constraints including precipitation and recharge events, lead to different recession parameters resulting both from the medium characteristics and the climate forcing (Figure 3). For this reason, we do not further consider estimates of recession constants from the analysis of the cloud and focus on the estimations drawn from single recessions analysis (per Jachens et al., 2020; Roques et al., 2017).

4.2 Spatial distribution and variability of storage-discharge functions

Our analysis revealed anomalous values of the constant of non-linearity in storage-discharge functions b_H andb_L measured at both high and low flows respectively (Figure 4). While the average b_H=3.06 fits with the theoretical prediction of b_H=3, values range from a minimum of 1.75 to a maximum of 6.91 across the catchments (Figure 4b). b_L measured at low flows appears to be systematically larger than b_H, ranging from 2.51 to 14.78 with an average of 5.58 (Figure 4a). This is inconsistent with what would be predicted from the classical thin homogeneous aquifer case following Boussinesq equations, pictured with a red circle in Figure 4b.

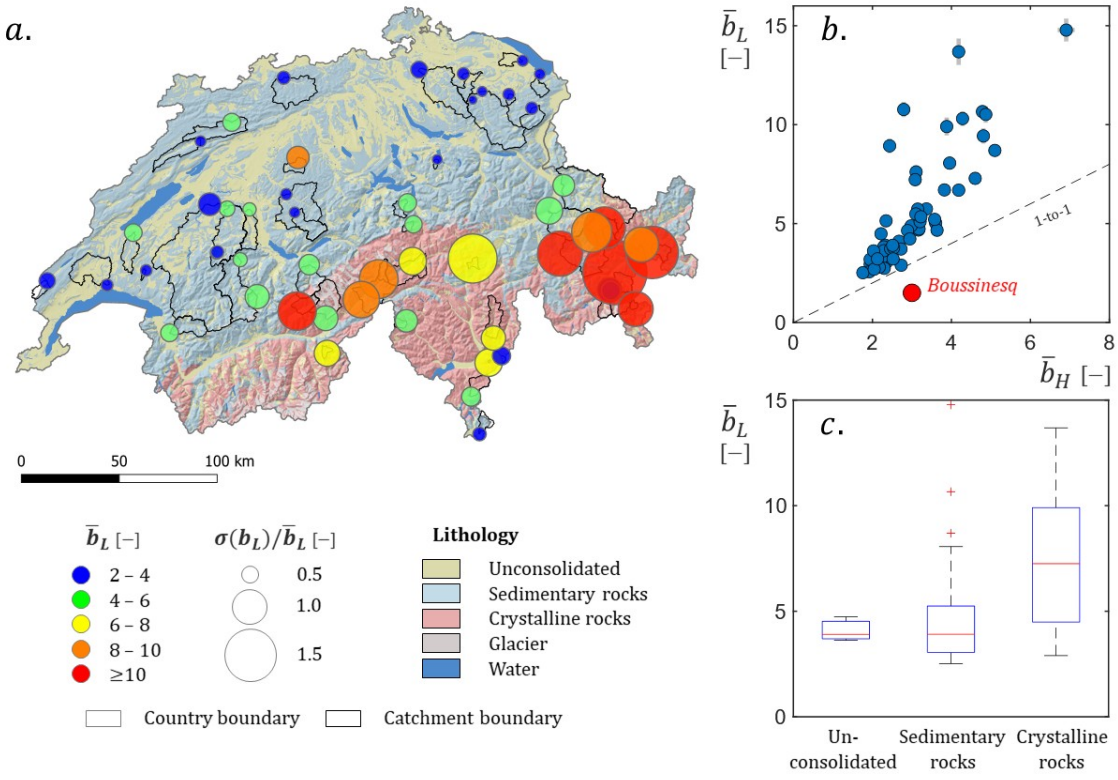

Figure 4. a) Spatial distribution of the mean constant of nonlinearity b_L pictured by circles with color scale from blue to red on top of the lithological map. The coefficient of variation $CV(b_L)=\sigma(b_L)/b_L$ is represented by the size of the disks, b) shows the mean constant of non-linearity for each catchment estimated at both high (b_H) and low (b_L) flow regimes. The grey error bars represent the standard errors. For reference, the values expected from the Boussinesq theory for thin homogeneous aquifers is drawn as a red disk. A clear positive correlation is observed with values systematically larger for

359 **recessions during low flows compared to the ones estimated at high flows. c) boxplot**
360 **representation of the distribution of b_L categorized by the dominant lithology.**

361 The spatial distribution of b_L and its coefficient of variation $CV(b_L)$ are mapped in Figure 4a.
362 Higher values of b_L were found in high alpine contexts settled in crystalline rocks (Figure 4c)
363 compared to the ones found in lower detritic plateaus. $CV(b_L)$ range from 50 to 150% with
364 the highest values also located in the high alpine crystalline rock regions. This is confirmed
365 by the statistical distribution of b_L for the main ensemble of lithologies (i.e. unconsolidated
366 sediments, sedimentary and crystalline rocks), where crystalline rocks have higher values of
367 b_L than unconsolidated sediments (Figure 4c).

368 ## 4.3 Ensemble correlation of recession constants with landscape
369 characteristics

370 Results of the statistical analysis are summarized in Figure 5. Figure 5a shows the main
371 groups of correlated variables in the 2 first components of the PCA, which explain 55% of
372 the total variance. In Figure 5b, we show part of the correlation matrix where the bubble size
373 scales with the Pearson's correlation coefficient and the colors highlight positive and negative
374 correlation in red and blue respectively. From this analysis, we identify the main hydrological
375 and geomorphological variables that are correlated and their degree of correlation:

376 1. Constant of non-linearity b_L and recession timescales τ are correlated with each other
377 and are aligned with the first Principal Component showing the first controlling factor
378 of variance in the dataset;
379 2. b_L and τ are strongly correlated with geological and geomorphological properties of
380 the landscapes, with a positive correlation with elevation, watershed slope, and
381 crystalline rocks coverage, and negatively correlated with depth to bedrock
382 (sedimentary cover), porosity and drainage density;
383 3. The coefficient of variation $CV(b_L)$ is correlated with the same set of parameters as
384 the average value of b_L and τ;

385 This analysis confirms that anomalously high values of b_L are observed in landscapes
386 dominated by crystalline rocks, high slopes, low drainage density and low depth to bedrock
387 while b_L tends toward lower values in flat landscapes dominated by unconsolidated sediments
388 and high drainage density.

We analyzed the structure of the correlations between the main hydrological parameters, i.e. b_L, $CV(b_L)$ and τ, with the geomorphological and geological characteristics of the catchments (Figure 6). We specifically focused on: 1) the average slope of the basin, 2) the drainage density, 3) the bedrock cover and 4) the depth to bedrock which controls most of the variance in our dataset (Figure 5).

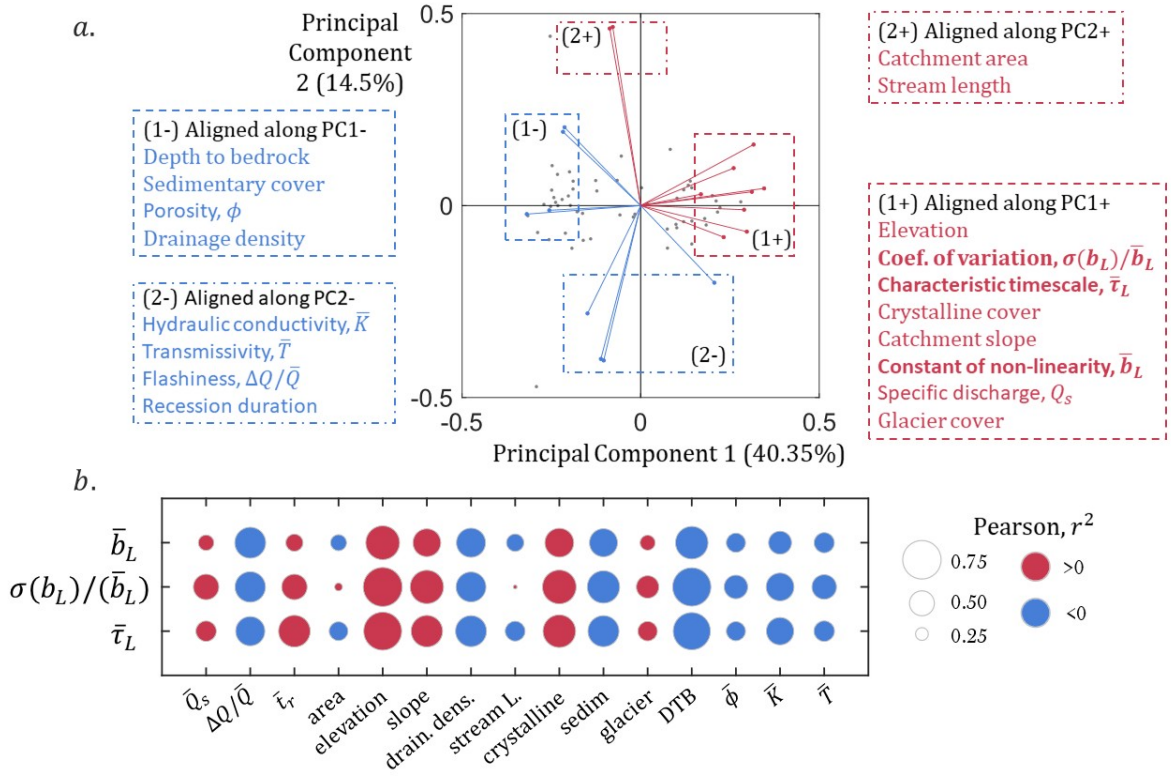

Figure 5. Results of the statistical analysis. In a) are displayed the 2 first components of the Principal Component Analysis (PCA), which explain 55% of the variance. The eigenvectors are grouped into 4 main categories according to the nature of their correlation, i.e. aligned with PC1 and PC2 and positively or negatively correlated. In b) is presented the correlation matrix of some of the parameters with the size of the bubbles scaled with the Pearson's coefficient and their colors revealing a positive (red) or negative (blue) correlation.

As expected, alpine landscapes with crystalline basements tend to have a higher average slope, less soil development (low depth to bedrock) and a lower drainage density; while landscapes settled in the valleys and plateaus with thick unconsolidated sediments present a much more developed river network. Hydrological behaviors for these two landscape end-members evolve from anomalous b_L with high variability in-between recessions toward lower values of b_L with low variability. These results highlight the strong control of landscape and

408 subsurface architectures on the average storage-discharge relationship from anomalous
409 hydrological behaviors in alpine crystalline settings, to behaviors described by homogeneous
410 aquifer theory (b_L=1.5) in systems dominated by detritic aquifers in valleys.

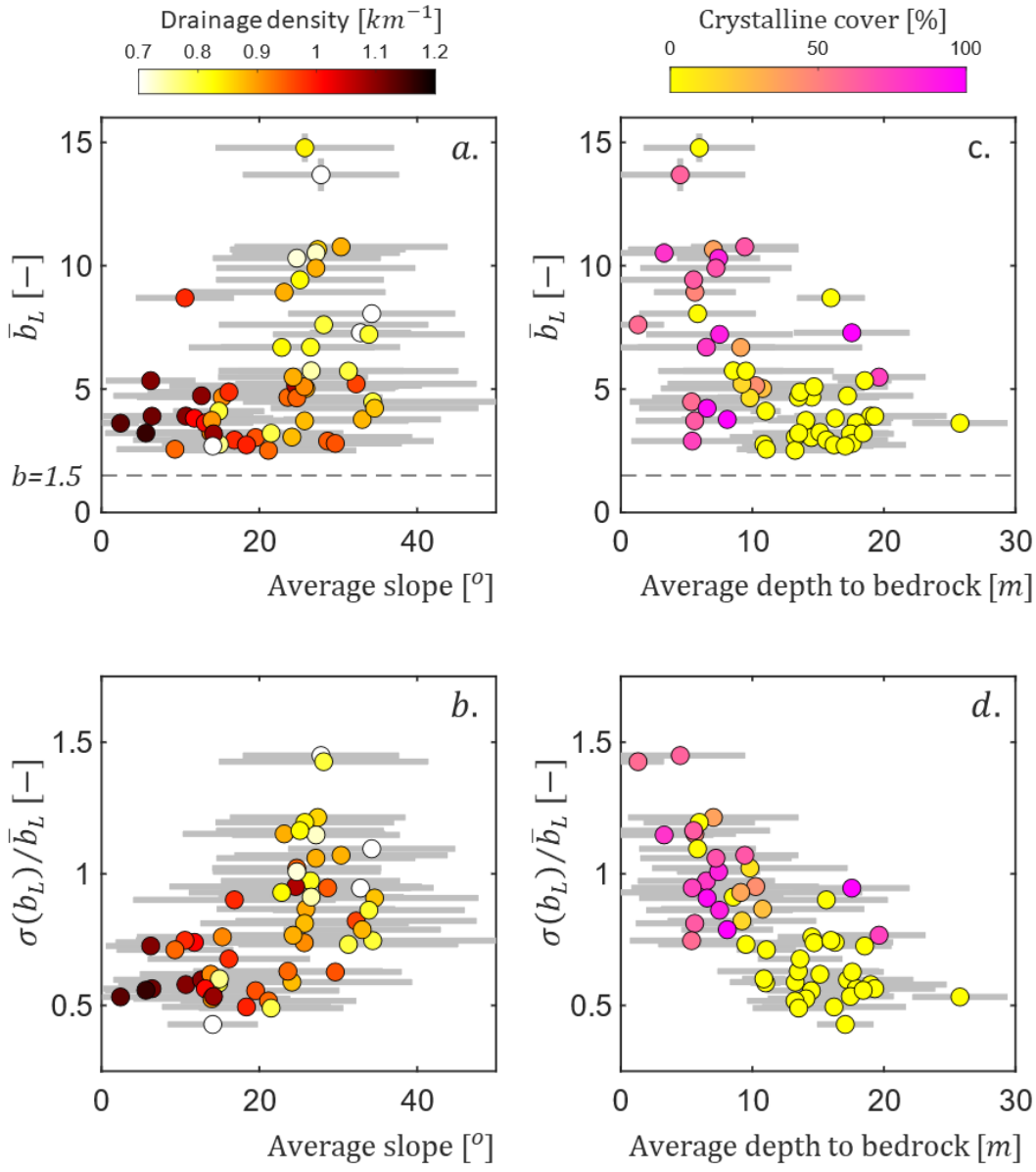

411

412 **Figure 6. Scatter plots showing the correlation between the constant of non-linearity b_L**
413 **(error bars show the standard errors) and its variability $\sigma(b_L)/b_L$ (organized as rows) as**
414 **a function of geomorphological (left column) and geological (right column) parameters.**
415 **a) b_L and b) $\sigma(b_L)/b_L$ vs average slope where symbols are color-coded according to the**
416 **drainage density; c) b_L and d) $\sigma(b_L)/b_L$ vs average depth to bedrock where symbols are**
417 **color-coded according to the proportion of crystalline rock cover. Error bars on the X**

axis show the standard deviation for the main geomorphological and geological parameters.

4.4 PREDICTION OF RECESSION TIMESCALES

τ is a critical parameter when evaluating the resilience of surface and groundwater resources as it contains both a geomorphological information, by scaling with the hillslope length L^2, and a geological information being inversely proportional to diffusivity D (Eq. 2). We found that effective diffusivities, estimated as L^2/τ, range over one order of magnitude from 5 10^{-2} to 6 10^{-1} m^2 s^{-1} (Figure 7a). This variability of values seems lower considering the variability in lithological and structural settings across the 54 selected catchments, largely independent of the catchment area sampled by the stream gauge (Figure 7a). From Figure 7a, we distinguished 2 groups of values that can be differentiated according to their lithology, in this case taken as the percentage of bedrock, with crystalline rocks globally showing lower diffusivities than other lithologies. This differentiation is expected as crystalline rocks tend to have lower permeability with respect to unconsolidated and sedimentary lithologies (Gleeson et al., 2014).

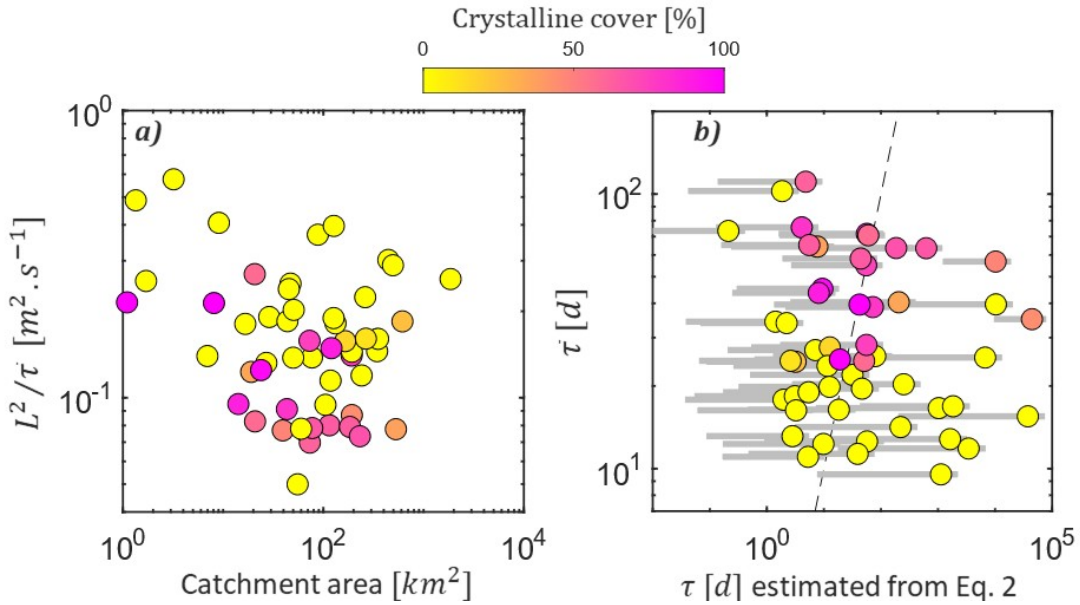

Figure 7. a) L^2/τ, proxy for hydraulic diffusivity $D[m^2/s]$, as a function of catchment area (error bars for Y axis are the standard errors), and, b) Average recession timescales estimated from single recession analysis (error bars for Y axis are the standard errors) vs diffusion timescales computed from Eq. 2 (Brutsaert, 1994)

accounting for the lithological interpolation of K and φ from the GLHYMPS database (Huscroft et al., 2018) (error bars for X axis illustrate the variability of τ computed for the range of K and φ available in the GLHYMPS database).

We also compared the values of estimated τ with those computed with Eq. 2 assuming a thick homogeneous aquifer with linearized Boussinesq flow solution (Figure 7b). Recession analysis revealed values of τ ranging from 10 to 110 days, with an average of 35 days. It is noteworthy to highlight that this 35-day timescale is close to that previously proposed as a representative estimate for effective groundwater parameters in several catchments (from 25 days in Brutsaert and Lopez (1998) to 45 +/- 15 days in Brutsaert (2008)), although those estimates were assessed with a different method (based on the lower envelope) than the one used here. However, Eq. 2 led to a much wider range of values, from 1 day to 104 days. While a few catchments are displayed along the 1:1 line, the vast majority shows strong deviations between observed and computed values. This result reveals the strong limitations of using Eq. 2 and effective hydraulic properties derived from a lithological database to estimate streamflow recession timescales at the catchment scale. Indeed, this assumption might fail in representing the complex architecture of groundwater flow involved in the subsurface.

5 DISCUSSION

Streamflow dynamics are controlled by numerous processes responsible for the transfer of water at the catchment scale. Groundwater plays the central role in this control, especially during baseflow periods, where the subsurface architecture shapes most of the dynamics and resilience of the system. Our analysis revealed unprecedented spatial and temporal variabilities in storage-discharge functions across the 54 selected catchments. This shows that groundwater contribution is not restricted to the drainage of a homogeneous reservoir, where the dynamics would be only controlled by effective hydraulic properties. This is confirmed by the strong deviation of the observed streamflow recession constants from the ones derived from analytical solutions considering homogeneous aquifers (Eq. 1 and 2). Here, we discuss the first-order landscape characteristics that may contribute to this deviation. We identify which types of landscape are likely to display anomalous storage-discharge functions and review current hypotheses regarding the main mechanisms that could be responsible.

469 5.1 GEOLOGICAL AND GEOMORPHOLOGICAL CONTROLS ON EFFECTIVE 470 DIFFUSION TIMESCALES

471 Landscapes display immense variability in morphological traits, resulting from the complex
472 interplay among tectonic, erosive, biospheric and anthropogenic forcings. The European Alps
473 constitutes a unique natural laboratory to explore this variability. Several tectonic and
474 lithological units can be distinguished, from the carbonates of the Jura Mountains, to the
475 Molasse basins and the crystalline basements of the Infrahelvetic complex and the overlying
476 Helvetic nappes (Kühni and Pfiffner, 2001; Schmid et al., 2004). These units have been
477 shaped by nine major glacial - interglacial cycles since the mid-Pleistocene Transition that
478 have triggered valley incision and glacial sediment output (Haeuselmann et al., 2007; Muttoni
479 et al., 2003), depositing sediments in the valley bottoms (Fox et al., 2015; Korup and
480 Schlunegger, 2007; Leith et al., 2018; Sternai et al., 2013; Valla et al., 2011). The present-day
481 Alps can be considered an immature mountain range in which local relief is significantly
482 greater than that which may be expected in a mature alpine setting, in which longitudinal
483 valley profiles reflect a balance between stream power and uplift rate, and hillslope gradients
484 are determined by that required for threshold sediment transport (Hergarten et al., 2010;
485 Howard and Kerby, 1983). As such, most catchments presented in this study are likely to
486 demonstrate characteristics consistent with environments in disequilibrium, including, steep
487 non-linear hillslopes, migrating drainage divides, fluvial knickpoints and waterfalls, bedrock
488 landslides, limited soil cover, and developing fracture networks consistent with strength-
489 limited hillslopes (Figure 8).

490 Theoretically, differences in effective timescales, τ, can be expected to be associated with the
491 variability in hydraulic properties of the rock mass, with τ proportional to $1/D = \varphi/(Ke)$
492 (Eq. 2), and the effective length of subsurface flow paths, with τ proportional to L^{2} (Eq. 2)
493 often estimated by the direct crest-to-stream distance, (L in figure 1). K, φ and L are all
494 constrained by the intrinsic mechanical properties of the rock mass: i.e. i) K and φ are
495 inversely proportional to the rock strength; and ii) landscapes with more competent rocks
496 tend to display larger valley spacing (Perron et al., 2009), and consequently larger L.
497 Although critical, the flowpath length L (Figure 1) is a more difficult metric to estimate than
498 a crest-to-stream distance. It depends directly on the geometric characteristics of the basin
499 and of the drainage network (wavelengths, shape, slopes) as well as on the distribution of
500 hydrodynamic properties in the subsurface. Both the geology and the morphology of the

basin shape the groundwater flow paths: the variety of lengths, the dimensionality of flow and its possible compartmentalization.

Our analysis revealed longer diffusion timescales for high alpine catchments while it appears significantly lower in catchments developed in structural valleys and plateaus. High elevation catchments are typically composed of low conductive and unweathered crystalline bedrock. Low conductive bedrock favors high water tables mostly following the topography, generating steep hydraulic gradients that favor both fast local flow and deeper paths through the bedrock (Gleeson and Manning, 2008; Haitjema and Mitchell-Bruker, 2005). However, catchments at lower elevations tend to be more compartmentalized with the development of soils and the presence of detritic deposits. This compartmentalization induces strong contrasts in diffusivity between aquifers which tend to concentrate fluxes in higher K and φ zones in the near surface (Figure 8).

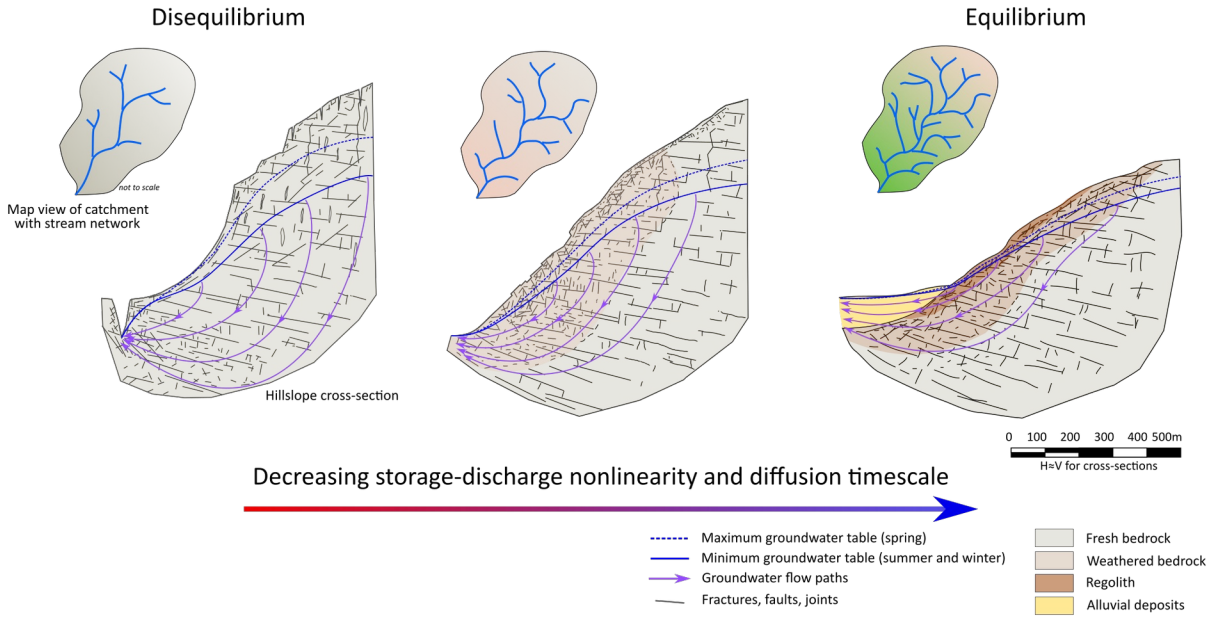

Figure 8. In this figure we show conceptual representations in 2D cross sections of the co-evolution between hillslope morphological and hydrological behavior in alpine settings with, on the left side, an example of glacier-dominated hillslope with steep slopes, low drainage density where groundwater flow is mostly dominated by a poorly diffusive fracture network with deep flow paths. This landscape shows high diffusion timescales and storage-discharge non-linearity. On the right side is presented a hillslope with typical fluvial features influenced by advanced erosion and weathering, where the stream network density increases. Groundwater is organized in shorter flow path

522 **lengths following the topography. This results in an evolution toward streamflow**
523 **recessions typical of drainage of thin homogeneous aquifers.**

524 The lithological constraint is classically used to calibrate the recession timescale τ. Our
525 estimations of aquifer diffusivity, approximated by L^2/τ (Figure 7a.), confirmed lower values
526 for crystalline-dominated catchments compared to the ones where detritic and sedimentary
527 formations are involved. In the meantime, we found several order of magnitudes differences
528 between the observed τ and the ones obtained analytically relying on the linearization of the
529 Boussinesq equation (Eq. 2) where average values of transmissivity and porosity are
530 extracted from global databases (Huscroft et al., 2018; Shangguan et al., 2017). While this
531 result highlights the strong limitations of i) the global databases in representing relevant
532 hydraulic properties to describe catchment scale processes, and, ii) the linear theory to
533 capture the groundwater flow complexity, such differences in the ranges of values spanning
534 several orders of magnitude was unexpected. From this result, we can argue that considering
535 the lithological constraints alone do not allow a full description of the complex interactions
536 between the subsurface and streamflow dynamics. The simplification of local
537 geomorphological, hydrogeological and climatic processes that might control the distribution
538 of flow paths introduce strong biases when estimating baseflow recession timescales and
539 sensitivity to drought.

540 5.2 HETEROGENEOUS LANDSCAPES LEAD TO ANOMALOUS STORAGE-
541 DISCHARGE RELATIONS

542 Anomalous values of b_L reflect strong non-linearities between storage and discharge
543 revealing potential controls from subsurface heterogeneity. The data presented in this work
544 show a gradient in the storage-discharge relation across the 54 catchments with high alpine
545 landscapes tending to have greater values of b_L than catchments located in the low-land
546 valleys and plateaus.

547 Landscapes are heterogeneous due to the organization of the topography (slope and hillslope
548 length distributions) and subsurface (permeability, porosity and compartmentalization). Slope
549 has been previously identified as a major driver for sustained low flows (Carlier et al., 2019,
550 2018) and higher b_L values (Karlsen et al., 2019; Mcmillan et al., 2014; Pauritsch et al., 2015;
551 Rupp and Selker, 2006) resulting from the combined effect of kinematic flow and steep
552 hydraulic gradients. Geology and subsurface heterogeneity exert additional controls on the

storage-discharge non-linearity in steep alpine catchments. Conceptually, anomalous storage-discharge functions can be explained by multiple linear reservoirs with different characteristic timescales (Perrin et al., 2003), where the degree on non-linearity scales with the variance in the distribution of τ (Harman et al., 2009). Our results suggest higher non-linearity in catchments dominated by unweathered bedrock at high elevation. In such context, groundwater flow and storage are controlled by a complex network of fractures and faults (Forster and Smith, 1988; Maillot et al., 2016; Welch and Allen, 2014) with an overall decreasing trend in hydraulic properties with depth (Achtziger-Zupančič et al., 2017; Rojstaczer et al., 2008). The strong variability in hydraulic properties, flow length and connectivity of the fractured bedrock favor high storage-discharge non-linearity. In addition, steep hillslopes might be subject to strong three-dimensional effects during drainage that might influence storage-discharge behavior, i.e. (1) stream network contraction in head basins during drainage (Biswal and Marani, 2010; Ghosh et al., 2016; Prancevic and Kirchner, 2019), and, (2) the rotation of flow length during drainage from perpendicular to parallel to the main stream channel controlled by hillslope angle with respect to stream slope. Both processes progressively increase the effective flow path length during drainage, which in turn increases the effective diffusion timescale (Jachens, 2020).

Moreover, catchments settled in weathered landscapes tend toward more homogeneous groundwater flow regimes. The development of fractures, soils and detritic aquifers in the near- surface with greater hydraulic conductivity concentrate groundwater flow, subparallel to the topography. In this configuration of simpler groundwater flow regimes, storage-discharge relations show lower non-linearity and lower drainage timescales (Figure 8).

While this convergence toward homogenization suggests that the assumption of Boussinesq flow could be valid, the dynamics of none of the 54 catchments analyzed here were well described with this assumption. Observed b_L from single recession analysis always deviated from the predictions established by the analytical solutions. Quantifying the relationship between aquifer compartmentalization, permeability architecture and storage-discharge behaviors at the catchment scale remains one of the main challenges in hydrology.

5.3 Initial conditions and memory effect during recharge contribute to the emergence of non-linear storage-discharge

Catchments with high storage-discharge nonlinearity, b_L, were located in high elevation bedrock catchments, and had higher coefficients of variation $CV(b_L)$. In these contexts, the storage-discharge behaviors are non-stationary and may change between recharge events. The initial conditions of saturation prevailing before the beginning of the recession might exert a strong impact in controlling the following discharge dynamics (Karlsen et al., 2019; Tashie et al., 2019). A conceptual explanation would suggest that, in a heterogeneous subsurface, groundwater flow is composed of a superposition of fast and slow drainage features, leading to complex recharge-storage- discharge superpositions between events (Harman et al., 2009; Jachens et al., 2020).

Alpine aquifers tend to include thick unsaturated zones, spanning over several tens to hundreds of meters (de Palézieux and Loew, 2019). In addition, low effective porosities of bedrocks favor strong seasonal variations of groundwater levels, mainly controlled by snowmelt recharge (Cochand et al., 2019; Manga, 1996; Safeeq et al., 2013; Somers and McKenzie, 2020). Assuming unconfined aquifers involved in a fractured bedrock, it means that the effective transmissivity can strongly and quickly evolve with the saturated thickness at the onset of drainage. It also implies that slow infiltration through the unsaturated zone might induce temporary storage that would be progressively released over long timescales (Luo et al., 2018; Rupp et al., 2009; Tashie et al., 2019; Wang, 2011). Those dynamic processes co-evolving during infiltration, saturated flow and discharge in Alpine bedrock catchments provides stream baseflow recession with a high variability in behaviors across recharge events.

5.4 Co-evolution of landscape morphology and hydrology: challenges for the representation of groundwater flow for large-scale modeling

Results revealed an unexpected diversity of streamflow behaviors across landscapes. They suggest that the spatial variability in drainage timescales and storage-discharge non-linearity are tightly linked to geomorphological contexts, for which first-order proxies, i.e. lithology, slope, drainage density and depth to bedrock, can be used to anticipate complex behaviors.

This co-evolution implies that consideration of properties associated with geomorphological maturity and / or equilibrium (e.g. relief, hillslope angle, soil formation, bedrock fracturing, and drainage patterns) and hydrological characteristics (stream network architecture and dynamics, hydraulic properties) cannot be disentangled if one aims at properly capturing the dynamics involved during the transfer of water, especially during baseflow regimes for which groundwater is the main contributor to stream discharge.

Predicting the resilience of landscapes to climate and anthropogenic modifications will then require an improvement in the manner in which groundwater-surface interactions are considered in numerical models (Clark et al., 2015). This raises a two-fold modeling challenge from considerations of different geologic and geomorphic settings:

1. How to inform the model of relevant storage-discharge relationships?
2. How to parametrize models with equivalent hydrodynamic properties of the subsurface that properly capture the dynamics?

Addressing these challenges requires:

1. building a global dataset describing the architecture of the subsurface (Fan et al., 2015), where depth to bedrock, catchment scale hydrodynamical parameters and anthropogenic pressures would complement the lithological description;
2. building global databases of hydrosystem behavior for wide ranges of geological, climatic and anthropogenic contexts, with homogeneous data and information, in order to apply systematic data analysis and test current models (eg. CAMELS dataset from Addor et al. (2017));
3. strengthening collaborations between communities involved in field and modeling activities for geomorphological, climatic and hydrological studies. These collaborations would allow the definition of relevant indicators and models to predict the processes involved at the interface between groundwater and surface water.

Such initiatives would contribute to better define coupled groundwater-river interactions within Earth System Models (Burek et al., 2020), focusing on the definition of pertinent sub-scale parametrization of lateral subsurface flow involved at the catchment scale.

PERSPECTIVES

In introductory courses in hydrology, geomorphology, and geology, we are all introduced to the idea that the landscape is a coupled system. We learn that water flowing through the landscape encounters, alters, and weathers rocks with different properties that, in turn, influence the pathways by which water flows through the landscape. We also learn that the movement of water through the landscape carves and shapes that landscape, and that the shape of the landscape, in turn, changes the way water moves. These concepts of landscapes evolving and co-evolving in response to these forcings underlie the emerging field of critical zone science (Brantley et al., 2011; Fan, 2015). Yet a coherent and comprehensive understanding of these linkages still awaits us, in large part because we are still searching for integrated models, both conceptual and physical, that allows us to recognize general principles that underlie the specific mechanisms and processes at work in any given landscape. The work reported here is only a start towards these more general principles, but we offer the evolutionary sequence shown in Fig. 8 as at least a testable hypothesis for how hydrological behavior might change over the course and timescales of landscape evolution. We look forward to the emergence of other competing hypotheses, and the tools and insights necessary to test alternative three-dimensional models of coupled hydrogeomorphic landscape trajectories.

ACKNOWLEDGEMENTS

All data supporting the conclusions can be freely obtained on national to global databases. Hydrological data can be obtained from the Federal Office for the Environment (FOEN) database: https://www.bafu.admin.ch/bafu/en/home/topics/water.html. Digital elevation model DHM25 of Switzerland can be obtained from the Federal Office of Topography https://www.swisstopo.admin.ch/ or alternatively on the Copernicus website: https://land.copernicus.eu/imagery-in-situ/eu-dem/eu-dem-v1.1. The global lithological dataset GLiM is detailed in Hartmann and Moosdorf (2012) and can be downloaded on https://doi.pangaea.de/10.1594/PANGAEA.788537. The global database GLHYMPS used to extract hydraulic properties of the subsurface is detailed in Huscroft et al. (2018) and available for download on https://dataverse.scholarsportal.info/dataset.xhtml?persistentId=doi:10.5683/SP2/DLGXYO. The Global Depth to Bedrock Dataset is described in Shangguan et al. (2017) and available for download on http://globalchange.bnu.edu.cn/ or http://soilgrids.org/.

672 Clément Roques would like to thank the Rennes Métropole research chair for funding his
673 research. Part of the funding comes from the National Science Foundation grant 1551483.
674 We acknowledge the support of SNO H+ network and OZCAR research infrastructure. The
675 authors would like to thank all colleagues who have contributed in shaping this work through
676 discussions and participation in field activities: Bjorn Bauhofer, Sarah Lewis, Cara Walter,
677 Bjorn Bauhofer, Anne Nolin, Simon Loew and many others.

678 ***REFERENCES***

679 Abbott, B.W., Bishop, K., Zarnetske, J.P., Minaudo, C., Chapin, F.S., Krause, S., Hannah,
680 D.M., Conner, L., Ellison, D., Godsey, S.E., Plont, S., Marçais, J., Kolbe, T., Huebner,
681 A., Frei, R.J., Hampton, T., Gu, S., Buhman, M., Sara Sayedi, S., Ursache, O., Chapin,
682 M., Henderson, K.D., Pinay, G., 2019. Human domination of the global water cycle
683 absent from depictions and perceptions. Nat. Geosci. 12, 533–540.
684 https://doi.org/10.1038/s41561-019-0374-y

685 Achtziger-Zupančič, P., Loew, S., Mariéthoz, G., 2017. A new global database to improve
686 predictions of permeability distribution in crystalline rocks at site scale. J. Geophys. Res.
687 Solid Earth 122, 3513–3539. https://doi.org/10.1002/2017JB014106

688 Addor, N., Newman, A.J., Mizukami, N., Clark, M.P., 2017. The CAMELS data set:
689 catchment attributes and meteorology for large-sample studies. Hydrol. Earth Syst. Sci.
690 21, 5293–5313. https://doi.org/10.5194/hess-21-5293-2017

691 Alley, W.M., Healy, R.W., LaBaugh, J.W., Reilly, T.E., 2002. Flow and storage in
692 groundwater systems. Science (80-.). 296, 1985–1990.
693 https://doi.org/10.1126/science.1067123

694 Andermann, C., Longuevergne, L., Bonnet, S., Crave, A., Davy, P., Gloaguen, R., 2012.
695 Impact of transient groundwater storage on the discharge of Himalayan rivers. Nat.
696 Geosci. 5, 127–132. https://doi.org/10.1038/ngeo1356

697 Berghuijs, W.R., Hartmann, A., Woods, R.A., 2016. Streamflow sensitivity to water storage
698 changes across Europe. Geophys. Res. Lett. 43, 1980–1987.
699 https://doi.org/10.1002/2016GL067927

700 Birsan, M.-V., Molnar, P., Burlando, P., Pfaundler, M., 2005. Streamflow trends in
701 Switzerland. J. Hydrol. 314, 312–329. https://doi.org/10.1016/j.jhydrol.2005.06.008

702 Biswal, B., Marani, M., 2010. Geomorphological origin of recession curves. Geophys. Res.
703 Lett. 37, 1–5. https://doi.org/10.1029/2010GL045415

704 Biswal, B., Nagesh Kumar, D., 2015. Estimation of "drainable" storage - A
705 geomorphological approach. Adv. Water Resour. 77, 37–43.
706 https://doi.org/10.1016/j.advwatres.2014.12.009

707 Blöschl, G., Bierkens, M.F.P., Chambel, A., Cudennec, C., Destouni, G., Fiori, A., Kirchner,
708 J.W., McDonnell, J.J., Savenije, H.H.G., Sivapalan, M., Stumpp, C., Toth, E., Volpi, E.,
709 Carr, G., Lupton, C., Salinas, J., Széles, B., Viglione, A., Aksoy, H., Allen, S.T., Amin,
710 A., Andréassian, V., Arheimer, B., Aryal, S.K., Baker, V., Bardsley, E., Barendrecht,
711 M.H., Bartosova, A., Batelaan, O., Berghuijs, W.R., Beven, K., Blume, T., Bogaard, T.,
712 Borges de Amorim, P., Böttcher, M.E., Boulet, G., Breinl, K., Brilly, M., Brocca, L.,
713 Buytaert, W., Castellarin, A., Castelletti, A., Chen, X., Chen, Yangbo, Chen, Yuanfang,
714 Chifflard, P., Claps, P., Clark, M.P., Collins, A.L., Croke, B., Dathe, A., David, P.C., de
715 Barros, F.P.J., de Rooij, G., Di Baldassarre, G., Driscoll, J.M., Duethmann, D., Dwivedi,
716 R., Eris, E., Farmer, W.H., Feiccabrino, J., Ferguson, G., Ferrari, E., Ferraris, S., Fersch,
717 B., Finger, D., Foglia, L., Fowler, K., Gartsman, B., Gascoin, S., Gaume, E., Gelfan, A.,
718 Geris, J., Gharari, S., Gleeson, T., Glendell, M., Gonzalez Bevacqua, A., González-
719 Dugo, M.P., Grimaldi, S., Gupta, A.B., Guse, B., Han, D., Hannah, D., Harpold, A.,
720 Haun, S., Heal, K., Helfricht, K., Herrnegger, M., Hipsey, M., Hlaváčiková, H.,
721 Hohmann, C., Holko, L., Hopkinson, C., Hrachowitz, M., Illangasekare, T.H., Inam, A.,
722 Innocente, C., Istanbulluoglu, E., Jarihani, B., Kalantari, Z., Kalvans, A., Khanal, S.,
723 Khatami, S., Kiesel, J., Kirkby, M., Knoben, W., Kochanek, K., Kohnová, S.,
724 Kolechkina, A., Krause, S., Kreamer, D., Kreibich, H., Kunstmann, H., Lange, H.,
725 Liberato, M.L.R., Lindquist, E., Link, T., Liu, J., Loucks, D.P., Luce, C., Mahé, G.,
726 Makarieva, O., Malard, J., Mashtayeva, S., Maskey, S., Mas-Pla, J., Mavrova-
727 Guirguinova, M., Mazzoleni, M., Mernild, S., Misstear, B.D., Montanari, A., Müller-
728 Thomy, H., Nabizadeh, A., Nardi, F., Neale, C., Nesterova, N., Nurtaev, B., Odongo,
729 V.O., Panda, S., Pande, S., Pang, Z., Papacharalampous, G., Perrin, C., Pfister, L.,
730 Pimentel, R., Polo, M.J., Post, D., Prieto Sierra, C., Ramos, M., Renner, M., Reynolds,
731 J.E., Ridolfi, E., Rigon, R., Riva, M., Robertson, D.E., Rosso, R., Roy, T., Sá, J.H.M.,
732 Salvadori, G., Sandells, M., Schaefli, B., Schumann, A., Scolobig, A., Seibert, J., Servat,
733 E., Shafiei, M., Sharma, A., Sidibe, M., Sidle, R.C., Skaugen, T., Smith, H., Spiessl,
734 S.M., Stein, L., Steinsland, I., Strasser, U., Su, B., Szolgay, J., Tarboton, D., Tauro, F.,

Thirel, G., Tian, F., Tong, R., Tussupova, K., Tyralis, H., Uijlenhoet, R., van Beek, R., van der Ent, R.J., van der Ploeg, M., Van Loon, A.F., van Meerveld, I., van Nooijen, R., van Oel, P.R., Vidal, J., von Freyberg, J., Vorogushyn, S., Wachniew, P., Wade, A.J., Ward, P., Westerberg, I.K., White, C., Wood, E.F., Woods, R., Xu, Z., Yilmaz, K.K., Zhang, Y., 2019. Twenty-three unsolved problems in hydrology (UPH) – a community perspective. Hydrol. Sci. J. 64, 1141–1158. https://doi.org/10.1080/02626667.2019.1620507

Brantley, S.L., Megonigal, J.P., Scatena, F.N., Balogh-Brunstad, Z., Barnes, R.T., Bruns, M.A., Van Cappellen, P., Dontsova, K., Hartnett, H.E., Hartshorn, A.S., Heimsath, A., Herndon, E., Jin, L., Keller, C.K., Leake, J.R., Mcdowell, W.H., Meinzer, F.C., Mozdzer, T.J., Petsch, S., Pett-Ridge, J., Pregitzer, K.S., Raymond, P.A., Riebe, C.S., Shumaker, K., Sutton-Grier, A., Walter, R., Yoo, K., 2011. Twelve testable hypotheses on the geobiology of weathering. Geobiology 9, 140–165. https://doi.org/10.1111/j.1472-4669.2010.00264.x

Brutsaert, W., 2008. Long-term groundwater storage trends estimated from streamflow records: Climatic perspective. Water Resour. Res. 44, 1–7. https://doi.org/10.1029/2007WR006518

Brutsaert, W., 1994. The unit response of groundwater outflow from a hillslope. Water Resour. Res. 30, 2759–2763. https://doi.org/10.1029/94WR01396

Brutsaert, W., Lopez, J.P., 1998. Basin-scale geohydrologic drought flow features of riparian aquifers in the Southern Great Plains. Water Resour. Res. 34, 233–240. https://doi.org/10.1029/97WR03068

Brutsaert, W., Nieber, J.L., 1977. Regionalized drought flow hydrographs from a mature glaciated plateau. Water Resour. Res. 13, 637–643. https://doi.org/10.1029/WR013i003p00637

Burek, P., Satoh, Y., Kahil, T., Tang, T., Greve, P., Smilovic, M., Guillaumot, L., Zhao, F., Wada, Y., 2020. Development of the Community Water Model (CWatM v1.04) – a high-resolution hydrological model for global and regional assessment of integrated water resources management. Geosci. Model Dev. 13, 3267–3298. https://doi.org/10.5194/gmd-13-3267-2020

Carlier, C., Wirth, S.B., Cochand, F., Hunkeler, D., Brunner, P., 2019. Exploring Geological

766 and Topographical Controls on Low Flows with Hydrogeological Models. Groundwater
767 57, 48–62. https://doi.org/10.1111/gwat.12845

768 Carlier, C., Wirth, S.B., Cochand, F., Hunkeler, D., Brunner, P., 2018. Geology controls
769 streamflow dynamics. J. Hydrol. 566, 756–769.
770 https://doi.org/10.1016/j.jhydrol.2018.08.069

771 Clara Santos, A., Manuela Portela, M., Rinaldo, A., Schaefli, B., 2018. Analytical flow
772 duration curves for summer streamflow in Switzerland. Hydrol. Earth Syst. Sci. 22,
773 2377–2389. https://doi.org/10.5194/hess-22-2377-2018

774 Clark, M.P., Bierkens, M.F.P., Samaniego, L., Woods, R.A., Uijlenhoet, R., Bennett, K.E.,
775 Pauwels, V.R.N., Cai, X., Wood, A.W., Peters-Lidard, C.D., 2017. The evolution of
776 process-based hydrologic models: Historical challenges and the collective quest for
777 physical realism. Hydrol. Earth Syst. Sci. 21, 3427–3440. https://doi.org/10.5194/hess-
778 21-3427-2017

779 Clark, M.P., Fan, Y., Lawrence, D.M., Adam, J.C., Bolster, D., Gochis, D.J., Hooper, R.P.,
780 Kumar, M., Leung, L.R., Mackay, D.S., Maxwell, R.M., Shen, C., Swenson, S.C., Zeng,
781 X., 2015. Improving the representation of hydrologic processes in Earth System Models.
782 Water Resour. Res. 51, 5929–5956. https://doi.org/10.1002/2015WR017096

783 Clark, M.P., Rupp, D.E., Woods, R.A., Tromp-van Meerveld, H.J., Peters, N.E., Freer, J.E.,
784 2009. Consistency between hydrological models and field observations: linking
785 processes at the hillslope scale to hydrological responses at the watershed scale. Hydrol.
786 Process. 23, 311–319. https://doi.org/https://doi.org/10.1002/hyp.7154

787 Cochand, M., Christe, P., Ornstein, P., Hunkeler, D., 2019. Groundwater Storage in High
788 Alpine Catchments and Its Contribution to Streamflow. Water Resour. Res. 55, 2613–
789 2630. https://doi.org/10.1029/2018WR022989

790 de Palézieux, L., Loew, S., 2019. Long-term transient groundwater pressure and deep
791 infiltration in Alpine mountain slopes (Poschiavo Valley, Switzerland). Hydrogeol. J.
792 27, 2817–2834. https://doi.org/10.1007/s10040-019-02025-9

793 Dralle, D.N., Karst, N.J., Charalampous, K., Veenstra, A., Thompson, S.E., 2017. Event-scale
794 power law recession analysis: Quantifying methodological uncertainty. Hydrol. Earth
795 Syst. Sci. 21, 65–81. https://doi.org/10.5194/hess-21-65-2017

796 Fan, Y., 2015. Groundwater in the Earth's critical zone: Relevance to large-scale patterns and
797 processes. Water Resour. Res. 51, 3052–3069. https://doi.org/10.1002/2015WR017037

798 Fan, Y., Clark, M., Lawrence, D.M., Swenson, S., Band, L.E., Brantley, S.L., Brooks, P.D.,
799 Dietrich, W.E., Flores, A., Grant, G., Kirchner, J.W., Mackay, D.S., McDonnell, J.J.,
800 Milly, P.C.D., Sullivan, P.L., Tague, C., Ajami, H., Chaney, N., Hartmann, A.,
801 Hazenberg, P., McNamara, J., Pelletier, J., Perket, J., Rouholahnejad−Freund, E.,
802 Wagener, T., Zeng, X., Beighley, E., Buzan, J., Huang, M., Livneh, B., Mohanty, B.P.,
803 Nijssen, B., Safeeq, M., Shen, C., Verseveld, W., Volk, J., Yamazaki, D., 2019.
804 Hillslope Hydrology in Global Change Research and Earth System Modeling. Water
805 Resour. Res. 55, 1737–1772. https://doi.org/10.1029/2018WR023903

806 Fan, Y., Richard, S., Bristol, R.S., Peters, S.E., Ingebritsen, S.E., Moosdorf, N., Packman, A.,
807 Gleeson, T., Zaslavsky, I., Peckham, S., Murdoch, L., Fienen, M., Cardiff, M., Tarboton,
808 D., Jones, N., Hooper, R., Arrigo, J., Gochis, D., Olson, J., Wolock, D., 2015.
809 DigitalCrust - a 4D data system of material properties for transforming research on
810 crustal fluid flow. Geofluids 15, 372–379. https://doi.org/10.1111/gfl.12114

811 Forster, C., Smith, L., 1988. Groundwater flow systems in mountainous terrain: 2.
812 Controlling factors. Water Resour. Res. 24, 1011–1023.
813 https://doi.org/10.1029/WR024i007p01011

814 Fox, M., Leith, K., Bodin, T., Balco, G., Shuster, D.L., 2015. Rate of fluvial incision in the
815 Central Alps constrained through joint inversion of detrital 10Be and
816 thermochronometric data. Earth Planet. Sci. Lett. 411, 27–36.
817 https://doi.org/10.1016/j.epsl.2014.11.038

818 Gaillardet, J., Braud, I., Hankard, F., Anquetin, S., Bour, O., Dorfliger, N., de Dreuzy, J.R.,
819 Galle, S., Galy, C., Gogo, S., Gourcy, L., Habets, F., Laggoun, F., Longuevergne, L., Le
820 Borgne, T., Naaim-Bouvet, F., Nord, G., Simonneaux, V., Six, D., Tallec, T., Valentin,
821 C., Abril, G., Allemand, P., Arènes, A., Arfib, B., Arnaud, L., Arnaud, N., Arnaud, P.,
822 Audry, S., Comte, V.B., Batiot, C., Battais, A., Bellot, H., Bernard, E., Bertrand, C.,
823 Bessière, H., Binet, S., Bodin, J., Bodin, X., Boithias, L., Bouchez, J., Boudevillain, B.,
824 Moussa, I.B., Branger, F., Braun, J.J., Brunet, P., Caceres, B., Calmels, D., Cappelaere,
825 B., Celle-Jeanton, H., Chabaux, F., Chalikakis, K., Champollion, C., Copard, Y., Cotel,
826 C., Davy, P., Deline, P., Delrieu, G., Demarty, J., Dessert, C., Dumont, M., Emblanch,
827 C., Ezzahar, J., Estèves, M., Favier, V., Faucheux, M., Filizola, N., Flammarion, P.,

828 Floury, P., Fovet, O., Fournier, M., Francez, A.J., Gandois, L., Gascuel, C., Gayer, E.,
829 Genthon, C., Gérard, M.F., Gilbert, D., Gouttevin, I., Grippa, M., Gruau, G., Jardani, A.,
830 Jeanneau, L., Join, J.L., Jourde, H., Karbou, F., Labat, D., Lagadeuc, Y., Lajeunesse, E.,
831 Lastennet, R., Lavado, W., Lawin, E., Lebel, T., Le Bouteiller, C., Legout, C., Lejeune,
832 Y., Le Meur, E., Le Moigne, N., Lions, J., Lucas, A., Malet, J.P., Marais-Sicre, C.,
833 Maréchal, J.C., Marlin, C., Martin, P., Martins, J., Martinez, J.M., Massei, N., Mauclerc,
834 A., Mazzilli, N., Molénat, J., Moreira-Turcq, P., Mougin, E., Morin, S., Ngoupayou,
835 J.N., Panthou, G., Peugeot, C., Picard, G., Pierret, M.C., Porel, G., Probst, A., Probst,
836 J.L., Rabatel, A., Raclot, D., Ravanel, L., Rejiba, F., René, P., Ribolzi, O., Riotte, J.,
837 Rivière, A., Robain, H., Ruiz, L., Sanchez-Perez, J.M., Santini, W., Sauvage, S.,
838 Schoeneich, P., Seidel, J.L., Sekhar, M., Sengtaheuanghoung, O., Silvera, N.,
839 Steinmann, M., Soruco, A., Tallec, G., Thibert, E., Lao, D.V., Vincent, C., Viville, D.,
840 Wagnon, P., Zitouna, R., 2018. OZCAR: The French Network of Critical Zone
841 Observatories. Vadose Zo. J. 17, 180067. https://doi.org/10.2136/vzj2018.04.0067

842 Gentine, P., Green, J.K., Guérin, M., Humphrey, V., Seneviratne, S.I., Zhang, Y., Zhou, S.,
843 2019. Coupling between the terrestrial carbon and water cycles - A review. Environ.
844 Res. Lett. 14. https://doi.org/10.1088/1748-9326/ab22d6

845 Ghosh, D.K., Wang, D., Zhu, T., 2016. On the transition of base flow recession from early
846 stage to late stage. Adv. Water Resour. 88, 8–13.
847 https://doi.org/10.1016/j.advwatres.2015.11.015

848 Gleeson, T., Manning, A.H., 2008. Regional groundwater flow in mountainous terrain:
849 Three-dimensional simulations of topographic and hydrogeologic controls. Water
850 Resour. Res. 44, 1–16. https://doi.org/10.1029/2008WR006848

851 Gleeson, T., Moosdorf, N., Hartmann, J., van Beek, L.P.H., 2014. A glimpse beneath earth's
852 surface: GLobal HYdrogeology MaPS (GLHYMPS) of permeability and porosity.
853 Geophys. Res. Lett. 41, 3891–3898. https://doi.org/10.1002/2014GL059856

854 Gleeson, T., Smith, L., Moosdorf, N., Hartmann, J., Dürr, H.H., Manning, A.H., Van Beek,
855 L.P.H., Jellinek, A.M., 2011. Mapping permeability over the surface of the Earth.
856 Geophys. Res. Lett. 38, 1–6. https://doi.org/10.1029/2010GL045565

857 Haeuselmann, P., Granger, D.E., Jeannin, P.Y., Lauritzen, S.E., 2007. Abrupt glacial valley
858 incision at 0.8 Ma dated from cave deposits in Switzerland. Geology 35, 143–146.

859 https://doi.org/10.1130/G23094A

860 Haitjema, H.M., Mitchell-Bruker, S., 2005. Are water tables a subdued replica of the
861 topography? Ground Water 43, 781–786. https://doi.org/10.1111/j.1745-
862 6584.2005.00090.x

863 Harman, C.J., Sivapalan, M., Kumar, P., 2009. Power law catchment-scale recessions arising
864 from heterogeneous linear small-scale dynamics. Water Resour. Res. 45, 1–13.
865 https://doi.org/10.1029/2008WR007392

866 Hartmann, A., Gleeson, T., Wada, Y., Wagener, T., 2017. Enhanced groundwater recharge
867 rates and altered recharge sensitivity to climate variability through subsurface
868 heterogeneity. Proc. Natl. Acad. Sci. U. S. A. 114, 2842–2847.
869 https://doi.org/10.1073/pnas.1614941114

870 Hartmann, J., Moosdorf, N., 2012. The new global lithological map database GLiM: A
871 representation of rock properties at the Earth surface. Geochemistry, Geophys.
872 Geosystems 13, 1–37. https://doi.org/10.1029/2012GC004370

873 Hergarten, S., Wagner, T., Stüwe, K., 2010. Age and Prematurity of the Alps Derived from
874 Topography. Earth Planet. Sci. Lett. 297, 453–460.
875 https://doi.org/10.1016/j.epsl.2010.06.048

876 Howard, A.D., Kerby, G., 1983. Channel changes in badlands. Geol. Soc. Am. Bull. 94, 739–
877 752. https://doi.org/10.1130/0016-7606(1983)94<739:CCIB>2.0.CO;2

878 Huscroft, J., Gleeson, T., Hartmann, J., Börker, J., 2018. Compiling and Mapping Global
879 Permeability of the Unconsolidated and Consolidated Earth: GLobal HYdrogeology
880 MaPS 2.0 (GLHYMPS 2.0). Geophys. Res. Lett. 45, 1897–1904.
881 https://doi.org/10.1002/2017GL075860

882 Jachens, E.R., 2020. Using Recession Analysis to Characterize Watershed Responses to
883 Drought. Oregon State University.

884 Jachens, E.R., Rupp, D.E., Roques, C., Selker, J.S., 2020. Recession analysis revisited:
885 Impacts of climate on parameter estimation. Hydrol. Earth Syst. Sci. 24, 1159–1170.
886 https://doi.org/10.5194/hess-24-1159-2020

887 Jefferson, A., Grant, G.E., Lewis, S.L., Lancaster, S.T., 2010. Coevolution of hydrology and
888 topography on a basalt landscape in the Oregon Cascade Range, USA. Earth Surf.

889 Process. Landforms 35, 803–816. https://doi.org/10.1002/esp.1976

890 Jung, M., Reichstein, M., Schwalm, C.R., Huntingford, C., Sitch, S., Ahlström, A., Arneth,
891 A., Camps-Valls, G., Ciais, P., Friedlingstein, P., Gans, F., Ichii, K., Jain, A.K., Kato,
892 E., Papale, D., Poulter, B., Raduly, B., Rödenbeck, C., Tramontana, G., Viovy, N.,
893 Wang, Y.-P., Weber, U., Zaehle, S., Zeng, N., 2017. Compensatory water effects link
894 yearly global land CO2 sink changes to temperature. Nature 541, 516–520.
895 https://doi.org/10.1038/nature20780

896 Karlsen, R.H., Bishop, K., Grabs, T., Ottosson-Löfvenius, M., Laudon, H., Seibert, J., 2019.
897 The role of landscape properties, storage and evapotranspiration on variability in
898 streamflow recessions in a boreal catchment. J. Hydrol. 570, 315–328.
899 https://doi.org/10.1016/j.jhydrol.2018.12.065

900 Kirchner, J.W., 2009. Catchments as simple dynamical systems: Catchment characterization,
901 rainfall-runoff modeling, and doing hydrology backward. Water Resour. Res. 45, 1–34.
902 https://doi.org/10.1029/2008WR006912

903 Kollet, S.J., Maxwell, R.M., 2006. Integrated surface-groundwater flow modeling: A free-
904 surface overland flow boundary condition in a parallel groundwater flow model. Adv.
905 Water Resour. 29, 945–958. https://doi.org/10.1016/j.advwatres.2005.08.006

906 Korup, O., Schlunegger, F., 2007. Bedrock landsliding, river incision, and transience of
907 geomorphic hillslope-channel coupling: Evidence from inner gorges in the Swiss Alps.
908 J. Geophys. Res. 112, F03027. https://doi.org/10.1029/2006JF000710

909 Kühni, A., Pfiffner, O.., 2001. The relief of the Swiss Alps and adjacent areas and its relation
910 to lithology and structure: topographic analysis from a 250-m DEM. Geomorphology
911 41, 285–307. https://doi.org/10.1016/S0169-555X(01)00060-5

912 Leith, K., Fox, M., Moore, J.R., 2018. Signatures of Late Pleistocene fluvial incision in an
913 Alpine landscape. Earth Planet. Sci. Lett. 483, 13–28.
914 https://doi.org/10.1016/j.epsl.2017.11.050

915 Liu, Y., Wagener, T., Beck, H.E., Hartmann, A., 2020. What is the hydrologically effective
916 area of a catchment? Environ. Res. Lett. 15, 104024. https://doi.org/10.1088/1748-9326/
917 aba7e5

918 Luo, Z., Shen, C., Kong, J., Hua, G., Gao, X., Zhao, Z., Zhao, H., Li, L., 2018. Effects of

919 Unsaturated Flow on Hillslope Recession Characteristics. Water Resour. Res. 54, 2037–
920 2056. https://doi.org/10.1002/2017WR022257

921 Maillot, J., Davy, P., Le Goc, R., Darcel, C., de Dreuzy, J.R., 2016. Connectivity,
922 permeability, and channeling in randomly distributed and kinematically defined discrete
923 fracture network models. Water Resour. Res. 52, 8526–8545.
924 https://doi.org/10.1002/2016WR018973

925 Manga, M., 1996. Hydrology of spring-dominated streams in the Oregon cascades. Water
926 Resour. Res. 32, 2435–2439. https://doi.org/10.1029/96WR01238

927 Mcmillan, H., Gueguen, M., Grimon, E., Woods, R., Clark, M., Rupp, D.E., 2014. Spatial
928 variability of hydrological processes and model structure diagnostics in a 50km2
929 catchment. Hydrol. Process. 28, 4896–4913. https://doi.org/10.1002/hyp.9988

930 Muttoni, G., Carcano, C., Garzanti, E., Ghielmi, M., Piccin, A., Pini, R., Rogledi, S.,
931 Sciunnach, D., 2003. Onset of major Pleistocene glaciations in the Alps. Geology 31,
932 989. https://doi.org/10.1130/G19445.1

933 Paniconi, C., Troch, P.A., Van Loon, E.E., Hilberts, A.G.J., 2003. Hillslope-storage
934 Boussinesq model for subsurface flow and variable source areas along complex
935 hillslopes: 2. Intercomparison with a three-dimensional Richards equation model. Water
936 Resour. Res. 39. https://doi.org/10.1029/2002WR001730

937 Pauritsch, M., Birk, S., Wagner, T., Hergarten, S., Winkler, G., 2015. Analytical
938 approximations of discharge recessions for steeply sloping aquifers in alpine
939 catchments. Water Resour. Res. 51, 8729–8740. https://doi.org/10.1002/2015WR017749

940 Perrin, C., Michel, C., Andréassian, V., 2003. Improvement of a parsimonious model for
941 streamflow simulation. J. Hydrol. 279, 275–289. https://doi.org/10.1016/S0022-
942 1694(03)00225-7

943 Perron, J.T., Kirchner, J.W., Dietrich, W.E., 2009. Formation of evenly spaced ridges and
944 valleys. Nature 460, 502–505. https://doi.org/10.1038/nature08174

945 Prancevic, J.P., Kirchner, J.W., 2019. Topographic Controls on the Extension and Retraction
946 of Flowing Streams. Geophys. Res. Lett. 46, 2084–2092.
947 https://doi.org/10.1029/2018GL081799

948 Rempe, D.M., Dietrich, W.E., 2014. A bottom-up control on fresh-bedrock topography under

949 landscapes. Proc. Natl. Acad. Sci. U. S. A. 111, 6576–6581.
950 https://doi.org/10.1073/pnas.1404763111

951 Richter, D. deB., Billings, S.A., 2015. 'One physical system': Tansley's ecosystem as Earth's
952 critical zone. New Phytol. 206, 900–912. https://doi.org/10.1111/nph.13338

953 Riebe, C.S., Hahm, W.J., Brantley, S.L., 2017. Controls on deep critical zone architecture: a
954 historical review and four testable hypotheses. Earth Surf. Process. Landforms 42, 128–
955 156. https://doi.org/10.1002/esp.4052

956 Rojstaczer, S.A., Ingebritsen, S.E., Hayba, D.O., 2008. Permeability of continental crust
957 influenced by internal and external forcing. Geofluids 8, 128–139.
958 https://doi.org/10.1111/j.1468-8123.2008.00211.x

959 Roques, C., Rupp, D.E., Selker, J.S., 2017. Improved streamflow recession parameter
960 estimation with attention to calculation of − dQ/dt. Adv. Water Resour. 108, 29–43.
961 https://doi.org/10.1016/j.advwatres.2017.07.013

962 Rupp, D.E., Schmidt, J., Woods, R.A., Bidwell, V.J., 2009. Analytical assessment and
963 parameter estimation of a low-dimensional groundwater model. J. Hydrol. 377, 143–
964 154. https://doi.org/10.1016/j.jhydrol.2009.08.018

965 Rupp, D.E., Selker, J.S., 2006. On the use of the Boussinesq equation for interpreting
966 recession hydrographs from sloping aquifers. Water Resour. Res. 42, 1–15.
967 https://doi.org/10.1029/2006WR005080

968 Rupp, D.E., Selker, J.S., 2005. Drainage of a horizontal Boussinesq aquifer with a power law
969 hydraulic conductivity profile. Water Resour. Res. 41, 1–8.
970 https://doi.org/10.1029/2005WR004241

971 Safeeq, M., Grant, G.E., Lewis, S.L., Tague, C.L., 2013. Coupling snowpack and
972 groundwater dynamics to interpret historical streamflow trends in the western United
973 States. Hydrol. Process. 27, 655–668. https://doi.org/10.1002/hyp.9628

974 Schaller, M.F., Fan, Y., 2009. River basins as groundwater exporters and importers:
975 Implications for water cycle and climate modeling. J. Geophys. Res. 114, D04103.
976 https://doi.org/10.1029/2008JD010636

977 Schmid, S.M., F�genschuh, B., Kissling, E., Schuster, R., 2004. Tectonic map and overall
978 architecture of the Alpine orogen. Eclogae Geol. Helv. 97, 93–117.

979 https://doi.org/10.1007/s00015-004-1113-x

980 Shangguan, W., Hengl, T., Mendes de Jesus, J., Yuan, H., Dai, Y., 2017. Mapping the global
981 depth to bedrock for land surface modeling. J. Adv. Model. Earth Syst. 9, 65–88. https://
982 doi.org/10.1002/2016MS000686

983 Shaw, S.B., Riha, S.J., 2012. Examining individual recession events instead of a data cloud:
984 Using a modified interpretation of dQ/dt-Q streamflow recession in glaciated watersheds
985 to better inform models of low flow. J. Hydrol. 434–435, 46–54. https://doi.org/10.1016/
986 j.jhydrol.2012.02.034

987 Somers, L.D., McKenzie, J.M., 2020. A review of groundwater in high mountain
988 environments. Wiley Interdiscip. Rev. Water 7, 1–27. https://doi.org/10.1002/wat2.1475

989 Sternai, P., Herman, F., Valla, P.G., Champagnac, J.D., 2013. Spatial and temporal variations
990 of glacial erosion in the RhÔne valley (Swiss Alps): Insights from numerical modeling.
991 Earth Planet. Sci. Lett. 368, 119–131. https://doi.org/10.1016/j.epsl.2013.02.039

992 Tashie, A., Pavelsky, T., Band, L.E., 2020. An Empirical Reevaluation of Streamflow
993 Recession Analysis at the Continental Scale. Water Resour. Res. 56, 1–18.
994 https://doi.org/10.1029/2019WR025448

995 Tashie, A., Scaife, C.I., Band, L.E., 2019. Transpiration and subsurface controls of
996 streamflow recession characteristics. Hydrol. Process. 33, 2561–2575.
997 https://doi.org/10.1002/hyp.13530

998 Taylor, R.G., Scanlon, B., Döll, P., Rodell, M., van Beek, R., Wada, Y., Longuevergne, L.,
999 Leblanc, M., Famiglietti, J.S., Edmunds, M., Konikow, L., Green, T.R., Chen, J.,
1000 Taniguchi, M., Bierkens, M.F.P., MacDonald, A., Fan, Y., Maxwell, R.M., Yechieli, Y.,
1001 Gurdak, J.J., Allen, D.M., Shamsudduha, M., Hiscock, K., Yeh, P.J.F., Holman, I.,
1002 Treidel, H., 2013. Ground water and climate change. Nat. Clim. Chang. 3, 322–329.
1003 https://doi.org/10.1038/nclimate1744

1004 Troch, P.A., Berne, A., Bogaart, P., Harman, C., Hilberts, A.G.J., Lyon, S.W., Paniconi, C.,
1005 Pauwels, V.R.N., Rupp, D.E., Selker, J.S., Teuling, A.J., Uijlenhoet, R., Verhoest,
1006 N.E.C., 2013. The importance of hydraulic groundwater theory in catchment hydrology:
1007 The legacy of Wilfried Brutsaert and Jean-Yves Parlange. Water Resour. Res. 49, 5099–
1008 5116. https://doi.org/10.1002/wrcr.20407

1009 Valla, P.G., Shuster, D.L., van der Beek, P.A., 2011. Significant increase in relief of the
1010 European Alps during mid-Pleistocene glaciations. Nat. Geosci. 4, 688–692.
1011 https://doi.org/10.1038/ngeo1242

1012 Wang, D., 2011. On the base flow recession at the Panola Mountain Research Watershed,
1013 Georgia, United States. Water Resour. Res. 47, 1–10.
1014 https://doi.org/10.1029/2010WR009910

1015 Welch, L.A., Allen, D.M., 2014. Hydraulic conductivity characteristics in mountains and
1016 implications for conceptualizing bedrock groundwater flow. Hydrogeol. J. 22, 1003–
1017 1026. https://doi.org/10.1007/s10040-014-1121-5

1018 Wood, E.F., Sivapalan, M., Beven, K., Band, L., 1988. Effects of spatial variability and scale
1019 with implications to hydrologic modeling. J. Hydrol. 102, 29–47.
1020 https://doi.org/10.1016/0022-1694(88)90090-X

1021 Yoshida, T., Troch, P.A., 2016. Coevolution of volcanic catchments in Japan. Hydrol. Earth
1022 Syst. Sci. 20, 1133–1150. https://doi.org/10.5194/hess-20-1133-2016

1023